

1 **Maximizing CRISPRi efficacy and accessibility with dual-sgRNA libraries and optimal**
2 **effectors**

3
4 Joseph M. Replogle^{1,4,†}, Jessica L. Bonnar^{2,4,†}, Angela N. Pogson^{2,4,†,‡}, Christina R. Liem^{2,‡},
5 Nolan K. Maier⁵, Yufang Ding⁵, Baylee J. Russell⁵, Xingren Wang⁵, Kun Leng^{1,6}, Alina Guna^{2,4},
6 Thomas M. Norman^{2,‡}, Ryan A. Pak^{2,‡}, Daniel M. Ramos^{7,8}, Michael E. Ward⁹, Luke A.
7 Gilbert^{2,10,11}, Martin Kampmann^{6,12}, Jonathan S. Weissman^{2-4,13,14,*}, Marco Jost^{2,5,*}

8
9 ¹Medical Scientist Training Program, University of California, San Francisco, San Francisco, CA
10 94158, USA

11 ²Department of Cellular and Molecular Pharmacology, University of California, San Francisco,
12 San Francisco, CA 94158, USA

13 ³Howard Hughes Medical Institute, Massachusetts Institute of Technology, Cambridge, MA
14 02142, USA

15 ⁴Whitehead Institute for Biomedical Research, Cambridge, MA 02142, USA

16 ⁵Department of Microbiology, Harvard Medical School, Boston, MA 02115, USA

17 ⁶Institute for Neurodegenerative Disease, University of California, San Francisco, San Francisco,
18 CA 94158, USA

19 ⁷Center for Alzheimer's Disease and Related Dementias, National Institutes of Health, Bethesda,
20 MD 20892, USA

21 ⁸National Institute on Aging, National Institutes of Health, Bethesda, MD 20892, USA

22 ⁹National Institute of Neurological Disorders and Stroke, NIH, Bethesda, MD 20892, USA

23 ¹⁰Department of Urology and Helen Diller Family Comprehensive Cancer Center, University of
24 California, San Francisco, CA 94158, USA

25 ¹¹Arc Institute, Palo Alto, CA, 94304, USA

26 ¹²Department of Biochemistry and Biophysics, University of California, San Francisco, San
27 Francisco, CA 94158, USA

28 ¹³Department of Biology, Massachusetts Institute of Technology, Cambridge, MA 02142, USA

29 ¹⁴David H. Koch Institute for Integrative Cancer Research, Massachusetts Institute of
30 Technology, Cambridge, MA 02142, USA

31

32 †Co-first authors

33 *Address correspondence to: J.S.W. (weissman@mit.edu); M.J. (marco_jost@hms.harvard.edu)

34

35 ‡Present Addresses:

36 Angela N. Pogson: Department of Developmental Biology, Stanford University School of
37 Medicine, Stanford, CA 94305, USA

38 Christina R. Liem: Division of Biological Sciences, Section of Cell and Developmental Biology,
39 University of California San Diego, La Jolla, CA 92093, USA

40 Ryan A. Pak: Department of Neuroscience, Scripps Research, La Jolla, CA 92037, USA

41 Thomas M. Norman: Computational & Systems Biology Program, Sloan Kettering Institute,
42 Memorial Sloan Kettering Cancer Center, New York, NY 10065, USA

43

44

45 **Abstract**

46 CRISPR interference (CRISPRi) enables programmable, reversible, and titratable repression of
47 gene expression (knockdown) in mammalian cells. Initial CRISPRi-mediated genetic screens
48 have showcased the potential to address basic questions in cell biology, genetics, and
49 biotechnology, but wider deployment of CRISPRi screening has been constrained by the large
50 size of single guide RNA (sgRNA) libraries and challenges in generating cell models with
51 consistent CRISPRi-mediated knockdown. Here, we present next-generation CRISPRi sgRNA
52 libraries and effector expression constructs that enable strong and consistent knockdown across
53 mammalian cell models. First, we combine empirical sgRNA selection with a dual-sgRNA
54 library design to generate an ultra-compact (1-3 elements per gene), highly active CRISPRi
55 sgRNA library. Next, we rigorously compare CRISPRi effectors to show that the recently
56 published Zim3-dCas9 provides the best balance between strong on-target knockdown and
57 minimal nonspecific effects on cell growth or the transcriptome. Finally, we engineer a suite of
58 cell lines with stable expression of Zim3-dCas9 and robust on-target knockdown. Our results and
59 publicly available reagents establish best practices for CRISPRi genetic screening.

60

61

62 **Introduction**

63 CRISPR interference (CRISPRi) enables programmable repression of gene expression with
64 broad applications in genome engineering, genetic screening, and cell biology (Doench, 2018).
65 In mammalian cells, CRISPRi requires two components: (i) an effector protein of catalytically
66 dead Cas9 (dCas9) fused to one or more transcription repressor domains, which recruits
67 endogenous epigenetic modulators to the genome, and (ii) a single guide RNA (sgRNA), which
68 directs the effector protein to target DNA (Gilbert et al., 2013). When the sgRNA is targeted to a
69 gene promoter, CRISPRi leads to repressive epigenome editing and knockdown of the gene
70 (Gilbert et al., 2014; Horlbeck et al., 2016a, 2016b).

71 Several features distinguish CRISPRi from Cas9 nuclease-mediated DNA cutting, the
72 major alternative CRISPR/Cas-based approach for loss-of-function genetic studies: i) Unlike
73 Cas9, CRISPRi does not rely on introduction of double-stranded DNA breaks and therefore does
74 not cause genomic rearrangements (Kosicki et al., 2018) and DNA damage-associated toxicity
75 (Meyers et al., 2017), which may be especially limiting in primary and stem cells (Bowden et al.,
76 2020; Haapaniemi et al., 2018; Ihry et al., 2018). ii) CRISPRi tends to confer more homogeneous
77 loss of gene function compared to Cas9, which often generates subpopulations of cells bearing
78 active in-frame indels (Smits et al., 2019). iii) CRISPRi is reversible and thus affords temporal
79 control over gene expression levels (Gilbert et al., 2014; Mandegar et al., 2016). iv) CRISPRi
80 enables titration of gene expression, which for example allows for partial depletion of genes
81 essential for cell growth and interrogation of the resulting phenotypes (Bosch et al., 2021;
82 Hawkins et al., 2020; Jost et al., 2020). v) In turn, one can directly measure the extent of on-
83 target knockdown as well as the corresponding responses in individual cells, for example using
84 single-cell RNA-seq (Perturb-seq), allowing for evaluation of the extent and potential biological
85 significance of cell-to-cell heterogeneity. vi) CRISPRi enables loss-of-function studies for non-
86 coding RNAs, which are difficult to inactivate or repress through CRISPR cutting and the
87 introduction of indels as they are insensitive to frame-shifting mutations (Liu et al., 2017).

88 Like other CRISPR approaches, CRISPRi has been paired with large-scale sgRNA
89 libraries to conduct systematic genetic screens. Such screens have been deployed to identify
90 essential protein-coding and non-coding genes (Gilbert et al., 2014; Haswell et al., 2021;
91 Horlbeck et al., 2016a; Liu et al., 2017; Raffeiner et al., 2020), to map the targets of regulatory
92 elements (Fulco et al., 2019, 2016; Gasperini et al., 2019; Kearns et al., 2015; Klann et al., 2017;

93 Thakore et al., 2015), to identify regulators of cellular signaling and metabolism (Coukos et al.,
94 2021; Liang et al., 2020; Luteijn et al., 2019; Semesta et al., 2020), to uncover stress response
95 pathways in stem cell-derived neurons (Tian et al., 2021, 2019), to uncover regulators of disease-
96 associated states in microglia and astrocytes (Dräger et al., 2022; Leng et al., 2022), to decode
97 regulators of cytokine production in primary human T-cells (Schmidt et al., 2022), to define
98 mechanisms of action of bioactive small molecules (Jost et al., 2017; Morgens et al., 2019; Sage
99 et al., 2017), to identify synthetic-lethal genetic interactions in cancer cells (Du et al., 2017;
100 Horlbeck et al., 2018), and to identify genetic determinants of complex transcriptional responses
101 using RNA-seq readouts (Perturb-seq) (Adamson et al., 2016; Replogle et al., 2022, 2020; Tian
102 et al., 2021, 2019), among others.

103 Despite these successes, two technical factors have limited wider adoption of CRISPRi.
104 First, CRISPRi screening is constrained by the large size of sgRNA libraries. Previous machine
105 learning efforts yielded guide design rules which substantially increased the activity of sgRNA
106 libraries (Horlbeck et al., 2016a; Sanson et al., 2018). Nonetheless, commonly used libraries
107 (e.g., Dolcetto, CRISPRi v2) target each gene with three or more sgRNAs to decrease false
108 negative results in screens. The development of a more compact, highly active sgRNA library
109 would enable CRISPRi screens in new cell types and for more complex phenotypes, especially
110 when cost, time, and/or cell numbers are limiting. Second, there is no clear consensus guiding
111 the use of the different reported CRISPRi effector proteins, complicating the generation of
112 CRISPRi cell models (Alerasool et al., 2020; Carleton et al., 2017; Gilbert et al., 2014; Yeo et
113 al., 2018).

114 Here we present a suite of tools to enable high-quality CRISPRi genetic screening in a
115 broad range of cell models. Based on empirical data aggregated from 126 screens, we design and
116 validate an ultra-compact, highly active CRISPRi library in which each gene is targeted by a
117 single library element encoding a dual sgRNA cassette. Next, we comprehensively compare
118 published CRISPRi effector proteins based on their on-target efficacy and non-specific effects on
119 transcription and cell proliferation. We find that the recently published Zim3-dCas9 provides the
120 best balance between strong on-target knockdown and minimal nonspecific effects. Finally, we
121 generate K562, RPE1, Jurkat, HT29, HuTu-80, and HepG2 cell lines engineered to stably
122 express Zim3-dCas9 and demonstrate robust on-target knockdown across these cell lines. Our
123 results and reagents establish best practices for CRISPRi genetic screening.

124
125
126
127
128
129
130
131
132
133
134
135
136
137
138
139
140
141
142
143
144
145
146
147
148
149
150
151
152
153

Results

Comparison of single and dual sgRNA CRISPRi libraries for genetic screening

A critical mediator of the potential applications of CRISPRi screening is the on-target efficacy and size of the sgRNA library. In recent work, we found that targeting individual genes with dual-sgRNA constructs substantially improved CRISPRi-mediated gene knockdown (Replogle et al., 2020). Building on this result, we asked whether a dual-sgRNA strategy could be used to generate an ultra-compact, genome-wide CRISPRi library.

To assess the potential utility of dual sgRNA libraries in systematic genetic screens, we began by cloning two pilot libraries for comparison: (i) one targeting each human gene with two distinct sgRNAs expressed from a tandem sgRNA cassette (dual sgRNA) and (ii) one targeting each human gene by only the single best sgRNA (see *Methods*; Table S1; Supplementary Note 1). We also optimized a protocol to amplify and sequence dual-sgRNA cassettes from lentivirally integrated genomic DNA (see *Methods*; Supplementary Note 2). Next, we compared the performance of our single- and dual-sgRNA libraries in a genome-wide growth screen (Figure 1A). We transduced K562 cells stably expressing dCas9-KRAB(Kox1) with our libraries, used puromycin to select for cells with lentiviral integration, and harvested cells at day 8 (T_0) and day 20 (T_{final}) post-transduction. We amplified sgRNA cassettes from extracted genomic DNA, sequenced to quantify sgRNA abundance in the two populations, and calculated growth phenotypes for each library element by comparing changes in abundance between T_0 and T_{final} (Figure 1C). The growth phenotypes produced by the single- and dual-sgRNA libraries were well-correlated with previously published CRISPRi growth screens using 5 sgRNAs per gene (single sgRNA $r = 0.81$; dual sgRNA $r = 0.82$; Figure S1A-C) and produced near-perfect recall of essential genes (Figure S1D) ($\text{AUC} > 0.98$ for both single- and dual-sgRNA libraries). Yet, for essential genes previously identified by the Cancer Dependency Map (DepMap) (Behan et al., 2019; Tsherniak et al., 2017), the dual-sgRNA library produced significantly stronger growth phenotypes (median 28% decrease in the growth rate $[\gamma]$) than the single-sgRNA library ($n = 1,847$ genes; single-sgRNA mean $\gamma = -0.19$; dual-sgRNA mean $\gamma = -0.24$; Mann Whitney p -value = $8 \cdot 10^{-13}$; Figure 1C, 1D), suggesting that the dual-sgRNA library confers stronger depletion of target genes.

154 A well-recognized challenge for the use of dual-sgRNA libraries is that the lentiviral
155 reverse transcriptase can undergo template switching between the two copies of the lentiviral
156 genome packaged into each capsid (Adamson et al., 2018, 2016; Feldman et al., 2018; Hill et al.,
157 2018; Horlbeck et al., 2018; Xie et al., 2018). These two copies generally bear two different
158 sgRNA pairs in a pooled dual-sgRNA library, such that template switching can produce a
159 recombined element with sgRNAs targeting different genes. Our sequencing strategy allowed us
160 to directly identify such recombined elements (Figure 1B), which occurred with a frequency of
161 29.4% across replicates, consistent with prior reports (Horlbeck et al., 2018; Replogle et al.,
162 2020). In our downstream analyses, we exclude all recombined elements such that they do not
163 impact phenotypes, although in principle these recombined elements could be used to assess
164 independent effects of the two sgRNAs targeting each gene.

165

166 *Design and validation of ultra-compact, dual sgRNA CRISPRi libraries*

167 Having validated the performance of dual-sgRNA libraries in a systematic genetic screen, we
168 sought to optimize the activity and utility of dual-sgRNA CRISPRi libraries (Figure 1E). To
169 optimize sgRNA selection for each gene, we aggregated empirical sgRNA activity data from 126
170 CRISPRi genetic screens (Table S2) and implemented a three-tiered selection system. First, for
171 genes that are essential in K562 cells, we ranked sgRNAs by growth phenotype. Second, for
172 genes that produced a significant phenotype in one of our previous CRISPRi screens, we ranked
173 sgRNAs by relative z-scored phenotype averaged across screens in which the target gene was
174 identified as a hit. Finally, for genes without any empirical effect in a prior screen, we ranked
175 sgRNAs according to predicted activities from the hCRISPRi v2.1 algorithm (see *Methods*)
176 (Horlbeck et al., 2016a). To allow users to select the library size suitable to their application, we
177 cloned sublibraries of the best single element (guide ranked 1+2; referred to as
178 hCRISPRi_dual_1_2), the second best element (guides ranked 3+4; referred to as
179 hCRISPRi_dual_3_4), or the third best element (guides ranked 5+6; referred to as
180 hCRISPRi_dual_5_6) (Table S3).

181 Further examination of the phenotypes from our screens revealed that a small number of
182 elements produced discordant effects between screens, which may arise from bottlenecking or
183 amplification bias (Figure S1A-C). For libraries with multiple elements targeting each gene, such
184 discordant effects can often be mitigated by comparing phenotypes across elements, but this

185 option is not available with single-element libraries. In previously reported CRISPR cutting
186 libraries, incorporation of barcodes into the sgRNA cassette enabled marking and tracing
187 populations of cells derived from individual lentiviral integrations, which allowed for detection
188 of bottlenecking events and amplification bias and thereby improved screen sensitivity and
189 robustness (Michlits et al., 2017; Zhu et al., 2019). Building on these results, we incorporated a
190 set of 215 8-nucleotide barcodes, which we term Integration Barcodes (IBCs), in the tandem
191 sgRNA cassette of our final hCRISPRi_dual_1_2, hCRISPRi_dual_3_4, and
192 hCRISPRi_dual_5_6 libraries (Methods, Table S4). We then optimized a sequencing strategy for
193 simultaneously sequencing the two sgRNAs, the IBC, and a sample index on Illumina
194 sequencers (Figure 1B, Supplementary Note 2).

195 Finally, we sought to test our optimized dual-sgRNA library side-by-side with the
196 recently reported Dolcetto CRISPRi library, which was designed with a differently prioritized
197 sgRNA selection algorithm and uses single-sgRNAs (Sanson et al., 2018). We used direct
198 capture Perturb-seq (Replogle et al., 2020), pooled CRISPR screens with single-cell RNA-seq
199 readout, to measure the on-target knockdown mediated by the top three elements in our dual
200 sgRNA library (guides 1+2, guides 3+4, or guides 5+6) or the three Dolcetto Set A sgRNAs for
201 128 randomly selected genes that are expressed in K562 cells (Table S5). Our dual-sgRNA
202 library significantly outperformed the Dolcetto library, as quantified by the average knockdown
203 (dual-sgRNA median knockdown 82%; Dolcetto median knockdown 65%; Mann Whitney p -
204 value = $2.4 \cdot 10^{-7}$) as well as the strongest knockdown per gene (dual-sgRNA median
205 knockdown 90%; Dolcetto median knockdown 87%; Mann Whitney p -value = $2 \cdot 10^{-4}$; Figure
206 1F). Indeed, the top-ranked element of our dual-sgRNA library (guides 1+2) alone produced
207 comparable knockdown to the best of all three Dolcetto sgRNAs (dual sgRNA element 1+2
208 median knockdown 86%; best Dolcetto sgRNA median knockdown 87%; Mann Whitney p -
209 value = 0.43) (Figure 1G). We note that an analogous dual-sgRNA approach may improve
210 knockdown for the Dolcetto library. Nonetheless, from these data we conclude that our dual-
211 sgRNA library improves on-target knockdown compared to gold-standard CRISPRi libraries.

212

213 *Design of CRISPRi effector expression constructs for systematic comparisons*

214 We next sought to compare different CRISPRi effectors, with the goal of identifying an effector
215 with strong activity and minimal non-specific effects on global transcription and cell growth. We

216 selected four repressor domains that had been described to mediate strong and specific
217 knockdown in dCas9 fusions: 1) the KRAB domain from KOX1 (*ZNF10*), which was used in the
218 original conception of CRISPRi (Gilbert et al., 2013); 2) the KRAB domain from ZIM3, which
219 was recently reported to mediate stronger knockdown than KRAB(KOX1) (Alerasool et al.,
220 2020); 3) the SIN3A interacting domain of MAD1 (SID4x) (Carleton et al., 2017); and 4) the
221 transcription repression domain of MeCP2 (Yeo et al., 2018).

222 To enable direct comparisons, we embedded each effector in a standardized lentiviral
223 expression construct (Figure 2A, Table S6). Briefly, in this construct, expression is driven by a
224 spleen focus-forming virus (SFFV) promoter, with an upstream ubiquitous chromatin opening
225 element (UCOE) to minimize silencing, internal nuclear localization signals (NLSs) and an
226 internal HA tag, a GFP marker linked at the C-terminus via a P2A ribosomal skipping sequence
227 to allow for stable cell line generation by FACS, and a Woodchuck Hepatitis Virus post-
228 transcriptional regulatory element (WPRES) in the 3' UTR to increase mRNA stability. Where
229 necessary, we included linker sequences derived from the functionally innocuous XTEN domain
230 (Schellenberger et al., 2009) to minimize proteolytic cleavage between dCas9 and fused
231 repressor domains. We attempted to maximize the activity for each repressor domain based on
232 our previous data and data in the literature, although we note that our evaluation is not
233 exhaustive. The final designs of the four effector expression constructs are depicted in Figure S2,
234 with further rationale in the Methods section. We then compared the four effectors with regards
235 to two key criteria: on-target activity and absence of non-specific effects on cell viability and
236 gene expression.

237
238 *CRISPRi effectors containing SID or MeCP2 domains have non-specific effects on cell viability*
239 *and gene expression*

240 The repressor domain of each CRISPRi effector is a transcription factor domain whose
241 overexpression has the potential to cause non-specific (i.e., not mediated by dCas9 targeting) and
242 potentially detrimental effects on transcription or cell proliferation. To test for effects on
243 proliferation, we generated K562 cell lines stably expressing each effector by lentiviral
244 transduction followed by FACS (Figure 2B) and then quantified the effect of each effector on
245 cell proliferation using an internally normalized competitive growth assay. We mixed cells
246 bearing each effector ~1:1 with cells expressing mCherry and quantified growth defects of

247 effector-expressing cells by measuring the ratio of mCherry-negative to mCherry-positive cells
248 over time by flow cytometry. We used mCherry-expressing cells as a reference population
249 instead of parental, GFP-negative cells because some of the effector-expressing cells convert to
250 GFP-negative over time due to silencing, which is difficult to separate from true dropout of
251 effector-expressing cells due to growth defects. Over 19 days, cells expressing dCas9 only,
252 dCas9-Kox1, or Zim3-dCas9 proliferated at the same rate as cells expressing GFP only or non-
253 transduced control cells, suggesting that expression of these effectors is not toxic over this time
254 span (Figure 2C). By contrast, cells expressing SID-dCas9-Kox1 had a strong growth defect
255 (~6% per day), and cells expressing dCas9-Kox1-MeCP2 had a mild growth defect (~1% per
256 day, Figure 2C).

257 To assess non-specific effects of effectors on transcription, we performed global
258 transcriptome profiling of K562 cells stably transduced with these effectors by RNA-seq (Figure
259 2D,E). Consistent with the growth assay, cells expressing SID-dCas9-Kox1 had globally
260 perturbed transcription, with 4282 genes differentially expressed compared to control cells
261 expressing GFP only at $p < 0.05$ (Figure 2E). Indeed, these samples clustered separately from
262 every other control and effector-expressing sample (Figure 2D). In addition, 53 genes were
263 differentially expressed in cells with dCas9-Kox1-MeCP2, suggesting that constitutive
264 expression of this effector also leads to minor non-specific effects on transcription (Figure 2E).
265 No more than 3 genes were detected to be differentially expressed in cells expressing any of the
266 other effectors, suggesting that these effectors do not non-specifically perturb transcription
267 (Figure 2E). Together, these results suggest that (over)expression of SID-dCas9-Kox1 is toxic
268 and globally perturbs transcription at least in K562 cells. We therefore excluded this effector
269 from further analysis.

270

271 *Zim3-dCas9 and dCas9-Kox1-MeCP2 mediate strongest knockdown*

272 We next sought to measure the efficacy of each effector in knocking down targeted genes with
273 two complementary approaches: (i) measurement of growth phenotypes resulting from
274 knockdown of essential genes, i.e. genes required for the growth or survival of dividing human
275 cells, and (ii) direct measurement of knockdown of cell surface proteins (Figure 3A, Table S7).
276 In both assays, we used single-sgRNA expression cassettes, which allowed us to use previously
277 validated strong and intermediate-activity sgRNAs (Jost et al., 2020). We included intermediate-

278 activity sgRNAs for two reasons: First, activity differences between effectors are more apparent
279 when knockdown is not saturated. Second, as it can be challenging to identify sgRNAs with high
280 activity across genes and cell types, effectors that mediate strong knockdown even with
281 imperfect sgRNAs could reduce false negative rates in genetic screens.

282 We measured growth phenotypes resulting from knockdown of essential genes using
283 internally normalized competitive growth assays. We transduced K562 cell lines stably
284 expressing each CRISPRi effector with vectors simultaneously expressing an sgRNA and a
285 fluorescent marker (mCherry) at a low multiplicity of infection (0.2-0.5). We then monitored the
286 ratio of sgRNA-expressing cells (mCherry+) and unperturbed cells (mCherry-) by flow
287 cytometry, with the expectation that cells with an essential gene-targeting sgRNA would deplete
288 at a rate proportional to CRISPRi activity. We targeted three genes, alanyl-tRNA synthetase
289 (*AARS*), the mitochondrial inner membrane import factor DNAJC19, and subunit D of RNA
290 polymerase I and III (*POLR1D*), with three different sgRNAs each. For all sgRNAs tested,
291 sgRNA-expressing cells depleted at the fastest rate with Zim3-dCas9 and at the second-fastest
292 rate with either dCas9-Kox1 or dCas9-Kox1-MeCP2 (Figures 3B, S3A).

293 Next, to directly measure depletion of targeted proteins, we knocked down the non-
294 essential cell surface proteins CD55 (complement decay-accelerating factor), CD81 (TAPA-1/
295 TSPAN28), and CD151 (TSPAN24) and measured staining intensity with fluorescently labeled
296 antibodies by flow cytometry as a proxy for protein levels. We transduced K562 lines stably
297 expressing the different CRISPRi effectors with vectors expressing either targeting or non-
298 targeting sgRNAs at a low multiplicity of infection (0.2-1). Six days after transduction, we
299 stained cells with fluorescently labeled antibodies against the different cell surface proteins and
300 assessed knockdown by comparing the median antibody staining intensity in cells expressing a
301 targeting sgRNA and cells expressing a non-targeting control sgRNA. With strong sgRNAs,
302 Zim3-dCas9, dCas9-Kox1, and dCas9-Kox1-MeCP2 all mediated strong depletion of each cell
303 surface protein (>96.8% median depletion for all effectors and sgRNAs). With weak sgRNAs,
304 dCas9-Kox1-MeCP2 mediated the strongest knockdown closely followed by Zim3-dCas9,
305 whereas dCas9-Kox1 mediated weaker knockdown (Figures 3C, 3D, S3B-D).

306 Importantly, flow cytometry reports on expression at the single-cell level, allowing us to
307 assess cell-to-cell heterogeneity in knockdown, which is missed when quantifying median
308 expression. As a proxy for heterogeneity, we calculated the fraction of cells without evidence of

309 knockdown despite the use of a strong sgRNA (Figure 3E). For Zim3-dCas9, knockdown was
310 largely homogeneous, with only ~5% of cells without detectable knockdown (Figures 3D, 3E,
311 S3B-D), perhaps due to the presence of some senescent cells in the population in which lack of
312 cell division limits protein dilution. By contrast, for dCas9-Kox1-MeCP2, 15-20% of cells did
313 not achieve knockdown (Figures 3D, 3E, S3B-D). This result may be explained by the toxicity of
314 the effector protein leading to selection against effector expression (Figure 2C) or may be
315 indicative of an intrinsic property of MeCP2 activity. The observed heterogeneity in MeCP2
316 knockdown may help explain why dCas9-Kox1-MeCP2 appears to mediate the strongest median
317 knockdown while Zim3-dCas9 leads to faster dropout of sgRNA-expressing cells in the essential
318 gene growth assay; in the growth assay, heterogeneity would lead to worse performance due to
319 selection against strong knockdown. In sum, these results suggest that the Zim3-dCas9 effector
320 confers strong knockdown that is homogeneous across a cell population.

321

322 *A versatile collection of Zim3-dCas9 constructs for robust knockdown across cell types*

323 To assess the general utility of the Zim3-dCas9 effector, we measured knockdown efficacy in
324 different cell types. For each cell type, we constructed cell lines stably expressing Zim3-dCas9
325 (see *Methods*; Supplementary Note 4) and measured knockdown of cell surface proteins by flow
326 cytometry. In both RPE1 (retinal pigment epithelium) and Jurkat (acute T-cell leukemia) cells,
327 cells expressing Zim3-dCas9 had stronger knockdown than previously reported cell lines
328 expressing dCas9-Kox1 (Figure 4A) (Horlbeck et al., 2018; Jost et al., 2017). Zim3-dCas9 also
329 conferred strong and homogeneous knockdown in HepG2 (hepatocellular carcinoma), HT29
330 (colorectal adenocarcinoma), and HuTu-80 (duodenal adenocarcinoma) cells (Figure 4B, S4).

331 To further maximize utility of the Zim3-dCas9 effector, we generated a panel of
332 constructs for expression of Zim3-dCas9 from the SFFV or EF1 α promoters linked to BFP, GFP,
333 or mCherry (Table S6). We also generated backbones to express effectors from additional
334 promoters (CMV, EFS) and with different types of C-terminal fluorescent protein linkages (P2A,
335 IRES, direct fusion) (Table S6). In addition, as the bright fluorescence from the fluorescent
336 proteins may be undesirable in some settings, we generated a construct in which expression of
337 Zim3-dCas9 is linked to a hygromycin resistance marker [Zim3-dCas9 (Hygro)]. K562 cells
338 stably transduced with Zim3-dCas9 (Hygro) and selected with hygromycin for 4 weeks had
339 strong and homogeneous knockdown that was indistinguishable from knockdown in a cell line

340 generated by FACS (Figure 4C). Finally, we generated constructs in which the fluorescent
341 protein is flanked by LoxP sites, such that the fluorescent protein can be removed by transient
342 delivery of Cre once a stable cell line has been generated (Table S6). All of our constructs are
343 available via Addgene. Our collection of Zim3-dCas9 expression constructs and streamlined
344 protocols enables robust CRISPRi across a broad range of cell models.

345

346 **Discussion**

347 High-quality genetic screening approaches are catalysts for basic research and drug development.
348 Among the available approaches, CRISPRi has several appealing features including
349 independence of double-stranded DNA breaks, homogeneity and reversibility of perturbations,
350 accessibility of partial loss-of-function phenotypes, and compatibility with direct measurements
351 of target gene expression levels in both bulk populations and single cells. CRISPRi screens have
352 indeed propelled biological discovery in several contexts, but broader deployment has been
353 limited by difficulties in generating CRISPRi cell models and limited knockdown efficacy for a
354 subset of genes. Here, we present a suite of tools and accompanying protocols to address these
355 limitations and improve the efficacy and accessibility of CRISPRi.

356 Our ultra-compact, dual-sgRNA CRISPRi library confers stronger knockdown and
357 growth phenotypes than previously reported libraries and thus should minimize false-negative
358 rates in screens. Nonetheless, this library also has drawbacks. First, some library elements
359 undergo intermolecular recombination during lentiviral transduction. We can detect and
360 computationally remove such recombination events, such that they do not corrupt the resulting
361 data. As a consequence, recombination primarily decreases effective library coverage, and in
362 return cell numbers need to be increased by ~20-30% to ensure coverage. In the future,
363 recombination may be further mitigated using decoy vectors, different promoters, and
364 alternatively processed guides (Adamson et al., 2016; Dong et al., 2017; Feldman et al., 2018;
365 Knapp et al., 2019). Second and perhaps more importantly, screens will be inherently noisier and
366 sensitive to off-target effects with only a single element per gene, such that in standard cell lines
367 in which cell numbers are not a concern, existing single-sgRNA libraries may remain the
368 approach of choice. Inclusion of the 3-4 and 5-6 element sublibraries in our dual-sgRNA library
369 can mitigate this noise at the expense of some of the compactness. In cases in which cell
370 numbers are limited by the model, time, or cost, however, the compactness of our dual-sgRNA

371 library will be transformative. Examples include screens in primary or stem-cell derived models
372 or *in vivo* as well as screens with high-content readout such as Perturb-seq (Bock et al., 2022;
373 Przybyla and Gilbert, 2021). Additionally, this dual-sgRNA strategy may provide similar
374 benefits for other CRISPR modalities such as CRISPR-mediated overexpression (CRISPR
375 activation, CRISPRa), as also described by others (Yin et al., 2022), and we have designed a
376 dual-sgRNA CRISPRa library for this purpose (Table S8). Finally, the improved knockdown
377 afforded by the dual-sgRNA approach will also be beneficial in arrayed experiments, in which
378 recombination is not a concern, and we have included a protocol for cloning dual-sgRNA
379 libraries in array (Supplementary Note 3). In sum, our dual-sgRNA libraries improve CRISPRi
380 knockdown and complement existing libraries by broadening the scope of models in which
381 CRISPRi screens are feasible.

382 In the realm of CRISPRi effectors, our work points to a clear consensus: Zim3-dCas9 is
383 the effector of choice, as it appears equal or superior to other effectors in every test we
384 performed and had no downsides. We had previously measured by Perturb-seq that Zim3-dCas9
385 afforded median mRNA knockdown of 91.6% across 2,285 genes in RPE1 cells (Replogle et al.,
386 2022), and here we further found that Zim3-dCas9 mediates robust knockdown across a range of
387 cell types. Our work highlights the importance of using multiple assays to assess effector
388 function including single-cell assays to assess cell-to-cell heterogeneity, of directly measuring
389 knockdown instead of relying on proxies such as growth phenotypes that conflate multiple
390 factors, and of evaluating effectors in stably transduced cells rather than in transiently transfected
391 cells to evaluate longer-term consequences for cell viability. To facilitate implementation of
392 CRISPRi in additional cell models, we created a suite of effector expression constructs with
393 different combinations of promoters and markers (Table S6) as well as a cell line generation
394 protocol (Supplementary Note 4).

395 Nonetheless, there is more progress to be made in evaluating effectors and generating
396 robust CRISPRi models. First, our comparison of the effectors was not exhaustive. For example,
397 although we expressed all effectors from the same context, we did not control for potential
398 differences in expression levels or nuclear localization across effectors. The Zim3-dCas9
399 expression constructs appear optimal as they are, but activities of other effectors may be boosted
400 by optimizing these factors. Second, repression of gene expression is generally mediated through
401 recruitment of endogenous cofactors; for KRAB domains such as those from Zim3 and Kox1,

402 this endogenous cofactor is TRIM28 (Ecco et al., 2017). TRIM28 expression varies by cell type,
403 and efficacy of Zim3 and Kox1 may be limited in cell types with low TRIM28 expression. In
404 such cell types, the MeCP2 effector may be a suitable alternative, but the selection against
405 effector-expressing cells may increase false positive and false negative rates. Third, we did not
406 measure if the effectors differed in propensity for sgRNA-dependent off-target effects. Previous
407 work on dCas9-Kox1 had documented that well-designed sgRNAs have minimal off-target
408 effects (Gilbert et al., 2013). The main source of off-target effects of CRISPRi are at
409 bidirectional promoters, which likely is an inevitable consequence of the mechanism of
410 CRISPRi. We note that the stronger activity of Zim3-based effectors may amplify such effects.
411 For now, such off-target effects can be readily predicted and measured, for example by Perturb-
412 seq (Replogle et al., 2022). Perhaps future efforts will identify strategies to limit knockdown of
413 neighboring genes. Finally, in some cell types effector expression is silenced over time, leading
414 to loss of CRISPRi activity. We described some strategies to counteract such silencing
415 (Supplementary Note 4), but further protection against silencing remains as an area for
416 improvement. In any case, the assays we describe may be used to test additional effectors in a
417 streamlined and standardized fashion, with the goal of making CRISPRi universally available
418 across cell models.

419 Altogether, our resources and best practices will guide both current implementations and
420 future developments of CRISPRi. All our protocols, constructs, cell lines, and libraries are
421 available as resources to the community.

422

423 **Acknowledgements**

424 We thank B. Adamson, J. Nuñez, J. Hussmann, M. Horlbeck, E. Chow, S. Gupta, and F. Urnov
425 for helpful discussions. We thank M. de Vera, S. Sinha, C. Muresan, and J. Kanter for lab and
426 administrative support. We thank I. Aifantis (NYU) for donating a vector containing SID4x and
427 G. Ow and E. Collisson (UCSF) for donating the mCherry-marked sgRNA expression vector.
428 We thank the UCSF Center for Advanced Technology for sequencing, the Whitehead Institute
429 Flow Cytometry Core and the Harvard Immunology Flow Cytometry Core Facility for access to
430 FACS machines and flow cytometers, and the Whitehead Institute Genome Technology Core for
431 performing bulk RNA-seq library preparation.

432

433 **Funding**

434 This work was supported in part by the National Institutes of Health (grants R00GM130964 to
435 MJ and RM1HG009490-01 to JSW), Springer Nature Global Grant for Gut Health 1772808
436 (MJ), a Charles H. Hood Foundation Child Health Research Award (MJ), DARPA HR0011-19-
437 2-0007 (JSW), the Ludwig Center at MIT (JSW), and the Chan Zuckerberg Initiative (JSW).
438 JMR was supported by NIH F31 Ruth L. Kirschstein National Research Service Award
439 NS115380. KL was supported by NIH F30 Ruth L. Kirschstein National Research Service
440 Award AG066418. BJR was supported by Harvard Bacteriology PhD Training Program T32
441 AI132120. AG was supported by Human Frontier Science Program grant 2019L/LT000858. MK
442 was supported by the Chan Zuckerberg Initiative Ben Barres Early Career Acceleration Award.
443 JSW is a Howard Hughes Medical Institute Investigator.

444

445 **Competing Interests**

446 JMR consults for Maze Therapeutics and Waypoint Bio. TMN consults for Maze Therapeutics.
447 MK serves on the Scientific Advisory Boards of Engine Biosciences, Casma Therapeutics, Cajal
448 Neuroscience, and Alektor, and is an advisor to Modulo Bio and Recursion Therapeutics.
449 MJ consults for Maze Therapeutics and Gate Bioscience. LAG declares outside interest in
450 Chroma Medicine. JSW declares outside interest in 5 AM Venture, Amgen, Chroma Medicine,
451 KSQ Therapeutics, Maze Therapeutics, Tenaya Therapeutics, Tessera Therapeutics, and Third
452 Rock Ventures. The Regents of the University of California with TMN, MJ, LAG, and JSW as
453 inventors have filed patent applications related to CRISPRi/a screening and Perturb-seq. LAG,
454 MK, and JSW are inventors on US Patent 11,254,933 related to CRISPRi/a screening.

455 **Data and Code Availability**

456 Python scripts for alignment of sequencing data from dual-sgRNA screens with and without
457 IBCs is available here: <https://github.com/josephreplogle/CRISPRi-dual-sgRNA-screens>.

458 Sequencing data are available on NCBI GEO under accession number GSE205310 (Perturb-seq)
459 and GSE205147 (bulk RNA-seq).

460

461 **Materials and Methods**

462 *Cell line generation and maintenance*

463 K562 cells were grown in RPMI 1640 medium with 25 mM HEPES, 2 mM L-glutamine, 2 g/L
464 NaHCO₃ (Gibco) supplemented with 10% (v/v) standard fetal bovine serum (FBS, VWR), 100
465 units/mL penicillin, 100 µg/mL streptomycin, and 2 mM L-glutamine (Gibco). hTERT-
466 immortalized RPE1 cells (ATCC, CRL-4000) were grown in DMEM:F12 (Gibco) supplemented
467 with 10% (v/v) standard FBS (VWR), 0.01 mg/mL hygromycin B, 100 units/mL penicillin, and
468 100 µg/mL streptomycin. Jurkat cells (ATCC, Clone E6-1 TIB-152) were grown in RPMI 1640
469 medium with 25 mM HEPES, 2 mM L-glutamine, 2 g/L NaHCO₃ (Gibco) supplemented with
470 10% (v/v) standard FBS (VWR), 100 units/mL penicillin, 100 µg/mL streptomycin, and 2 mM L-
471 glutamine (Gibco). HepG2 and HuTu-80 cells (both ATCC) were grown in Eagle's Minimum
472 Essential Medium with 1.5 g/L NaHCO₃, 110 mg/L sodium pyruvate, 292 mg/L L-glutamine
473 (Corning) supplemented with 10% (v/v) standard FBS (R&D Systems), 100 units/mL penicillin,
474 and 100 µg/mL streptomycin (Gibco). HT29 cells (ATCC) were grown in DMEM with 25 mM
475 D-glucose, 3.7 g/L NaHCO₃, 4 mM L-glutamine (Gibco) supplemented with 10% (v/v) standard
476 FBS (R&D Systems), 100 units/mL penicillin, and 100 µg/mL streptomycin (Gibco). HEK293T
477 cells were grown in Dulbecco's modified eagle medium (DMEM) with 25 mM D-glucose, 3.7
478 g/L NaHCO₃, 4 mM L-glutamine (Gibco) and supplemented with 10% (v/v) standard FBS (VWR
479 or R&D Systems), 100 units/mL penicillin, 100 µg/mL streptomycin, and 2 mM L-glutamine
480 (Gibco). K562 (chronic myelogenous leukemia) and HT29 (colorectal adenocarcinoma) cells are
481 derived from female patients. Jurkat (acute T-cell leukemia), HuTu-80 (duodenal
482 adenocarcinoma), and HepG2 (hepatocellular carcinoma) cells are derived from male patients.
483 HEK293T (embryonic kidney) cells are derived from a female fetus. RPE1 (immortalized retinal
484 pigment epithelium) cells are derived from a female subject. All cell lines were grown at 37 °C
485 in the presence of 5% CO₂.

486 To generate the K562 cell lines stably expressing various CRISPRi effectors, parental
487 K562 cells were stably transduced with lentiviral vectors expressing the corresponding effectors
488 linked to GFP via a P2A ribosome skipping sequence from an SFFV promoter with an upstream
489 ubiquitous chromatin opening element (UCOE). Polyclonal populations of GFP-positive cells
490 were selected using two rounds of fluorescence-activated cell sorting (FACS) on a Sony SH800S
491 Cell Sorter.

492 To generate RPE1 cells stably expressing Zim3-dCas9, RPE-1 cells were infected with
493 lentivirus containing UCOE-SFFV-Zim3-dCas9-P2A-BFP (pJB108) at low multiplicity of
494 infection by centrifugation at $1000 \times g$. Polyclonal populations of BFP-positive cells were
495 selected using two rounds of FACS on a Sony SH800S Cell Sorter. To generate Jurkat cells
496 stably expressing Zim3-dCas9, Jurkat cells were infected with virus containing UCOE-EF1 α -
497 Zim3-dCas9-P2A-mCh (pJB109) at low multiplicity of infection by centrifugation at $1000 \times g$.
498 Polyclonal populations of mCherry-positive cells were selected using two rounds of FACS on a
499 Sony SH800S Cell Sorter. To generate HepG2, HuTu-80, and HT29 cells stably expressing
500 Zim3-dCas9, cells were infected with lentivirus containing UCOE-EF1 α -Zim3-dCas9-P2A-mCh
501 (pJB109) at low multiplicity of infection. Polyclonal populations of mCherry-positive cells were
502 selected using two rounds of FACS on a FACSAria II Cell Sorter (BD Biosciences). To generate
503 K562 cells stably expressing Zim3-dCas9 without a fluorescent marker, K562 cells were infected
504 with virus containing UCOE-SFFV-Zim3-dCas9-P2A-hygro (pAG389) at low multiplicity of
505 infection by centrifugation at $1000 \times g$. To select for a polyclonal population, cells were treated
506 48 hours after infection with 200 $\mu\text{g}/\text{mL}$ hygromycin for one week, followed by treatment 500
507 $\mu\text{g}/\text{ml}$ hygromycin for three weeks.

508

509 *Lentivirus production*

510 Lentivirus was generated by transfecting HEK239T cells with the transfer plasmid and four
511 packaging plasmids (for expression of VSV-G, Gag/Pol, Rev, and Tat) using TransIT-LT1
512 Transfection Reagent (Mirus Bio). Viral supernatant was harvested two days after transfection
513 and filtered through 0.44 μm PES filters and/or frozen at -80°C prior to transduction.

514

515 *Design and cloning of pilot genome-wide single- and dual-sgRNA CRISPRi libraries*

516 To compare the use of single- and dual-sgRNA CRISPRi libraries in systematic genetic screens,
517 pilot genome-wide single- and dual-sgRNA CRISPRi libraries were designed and cloned.
518 sgRNAs targeting each gene were selected from our previously published hCRISPRi v2 library
519 by balancing empirical data from previous genetic screens with Horlbeck *et al.* predicted
520 rankings (Horlbeck et al., 2016a) using a three-tiered approach:

521 Tier 1. For genes essential for growth in the K562 CRISPRi screen data (p -value < 0.001
522 and $\gamma < -0.2$) (Horlbeck et al., 2016a), sgRNAs were ranked by their growth phenotype.

523 Tier 2. As many genetic perturbations only cause a conditional cellular phenotype (e.g.,
524 in a particular cell type, chemical stressor, or reporter phenotype), we next aggregated data
525 across multiple genetic screens (only a subset of the data in Table S2 was available for the pilot
526 library design). For genes that were identified as a significant hit [FDR 0.05 based on MAGeCK
527 RRA p -value (Li et al., 2014)] in previous CRISPRi screens, sgRNAs were ranked by the sum of
528 z -scored phenotypes across screens.

529 Tier 3. For all other genes, sgRNAs were ranked by the regression scores in hCRISPRi
530 v2.1 (Horlbeck et al., 2016a).

531 Using this ranking scheme, we selected the single best sgRNA for a single-
532 sgRNA/single-element-per-gene library (dJR004) and the two best sgRNAs for a dual-
533 sgRNA/single-element-per-gene library (dJR020). A list of sgRNA targeting sequences both the
534 single and dual sgRNA libraries is available in Table S1.

535 The single-sgRNA library dJR004 was cloned using the protocol described here:
536 https://weissman.wi.mit.edu/resources/Pooled_CRISPR_Library_Cloning.pdf. A modified
537 CROP-seq sgRNA lentiviral expression vector (pJR107) was derived from the parental vector
538 pBA950 (<https://www.addgene.org/122239/>) by incorporating a GFP fluorescent marker and a
539 UCOE element upstream of the EF1alpha promoter to prevent marker silencing. sgRNA
540 targeting sequences were appended with flanking sequence, BstX1/BlpI overhangs, and PCR
541 adapters. The library was synthesized as an oligonucleotide pool (Twist Biosciences), PCR-
542 amplified, BstX1/BlpI-digested, and inserted into pJR107 by ligation.

543 The dual-sgRNA library dJR020 was cloned using the protocol in Supplementary Note 1.
544 Briefly, dual-sgRNA targeting sequences were spaced by a BsmBI-cut site and appended with
545 flanking sequence, BstX1/BlpI overhangs, and PCR adapters with the structure: with the
546 structure: 5'- PCR adaptor - CCACCTTGTTG – targeting sequence A -

547 gtttcagagcgagacgtgcctgcaggatacgtctcagaaacatg – targeting sequence B -
548 GTTTAAGAGCTAAGCTG - PCR adaptor-3'. The library was synthesized as an
549 oligonucleotide pool (Twist Biosciences), PCR-amplified, BstX1/BlpI-digested, and inserted into
550 pJR104 by ligation. Next, the sgRNA CR3/hU6 promoter insert pJR98 was BsmBI-digested and
551 ligated into the BsmBI-digested library to generate the final library. In the final library, each
552 element expresses two unique sgRNAs from tandem U6 expression cassettes.

553

554 *Genome-wide growth screens for library comparison*

555 Parallel growth screens were performed to compare dJR004 versus dJR020. Lentivirus from
556 dJR004 and dJR020 was produced in HEK293T as described above. CRISPRi K562 cells
557 expressing dCas9-KOX1 KRAB were spininfected (1000G) with polybrene (8 ug/ml) with lentivirus
558 from dJR004 and dJR020 in biological replicate. Throughout the screen, cells were maintained at
559 a density between 250,000 – 1,000,000 cells per ml and 1000X coverage per library element. On
560 day 3 post-transduction, an infection rate of 11%-18% was measured by GFP fluorescence. On
561 day 3 through day 6 post-transduction, puromycin at 1 ug/ml was used to select for infected cells,
562 and cells were allowed to recover for two days. On day 8 post-transduction, a cell pellet was frozen
563 for each replicate representing the initial sample (T_0) of the screen. Throughout the screen, the
564 number of cell doublings was recorded, and final samples (T_{final}) were collected on day 20 post-
565 transduction.

566

567 *Screen library preparation, sequencing, and analysis*

568 Amplicon DNA libraries were prepared from cell pellets as previously described (Nuñez et al.,
569 2021). Genomic DNA was isolated using a NucleoSpin Blood XL kit or NucleoSpin Blood L kit
570 (Macherey–Nagel) depending on pellet size. Purified genomic DNA was directly amplified by
571 22 cycles of PCR using NEBNext Ultra II Q5 PCR MasterMix (NEB). Sequencing was
572 performed on a NovaSeq 6000 (Illumina) using a 19 bp Read 1, 19 bp Read 2, and 5 bp Index
573 Read 1 with custom sequencing primers.

574 After sequencing, sgRNA sequencing reads were aligned to the single and dual sgRNA
575 libraries using a custom Python script without allowing mismatches. Reads for which the Read 1
576 and Read 2 sgRNA sequences did not target the same gene likely arose from lentiviral
577 recombination and were discarded from downstream analysis. For both replicates of the dual-

578 sgRNA library, 29.4%, of mapped reads contained sgRNAs targeting different genes. For each
579 sgRNA or sgRNA pair, the growth phenotype was defined as the $\log_2(\text{sgRNA count } T_{\text{final}} /$
580 $\text{sgRNA count } T_0) - \text{median non-targeting control } \log_2(\text{sgRNA count } T_{\text{final}} / \text{sgRNA count } T_0)$
581 divided by the replicate total cell doublings (Gilbert et al., 2014). For the analysis of the Cancer
582 Dependency Map (DepMap) Common Essential genes, the 20Q1 Common Essential genes were
583 downloaded from <https://depmap.org/portal/download/>. For receiver operating characteristic
584 (ROC) curve analysis, “positives” were defined as genes with a K562 CRISPRi growth screen p -
585 value < 0.001 and $\gamma < -0.05$ (Horlbeck et al., 2016a), and “negatives” were defined as non-
586 targeting control guide pairs.

587

588 *Empirical sgRNA selection, incorporation of integration barcodes, and validation of finalized*
589 *dual-sgRNA CRISPRi libraries*

590 While the pilot dual-sgRNA library dJR020 enabled validation of the dual-sgRNA strategy,
591 finalized dual-sgRNA libraries were designed with additional considerations. An expanded set of
592 aggregated CRISPR screen data was used to optimize guide selection (Table S2). Optimal
593 sgRNAs targeting each gene were selected using an updated set of rules. First, sgRNAs
594 containing a BsmBI target sequence (CGTCTC or GAGACG) were removed to avoid dropout
595 during cloning. Second, each transcript per gene in Horlbeck *et al.*, 2016a was targeted
596 independently. Genes were separated into three tiers, similar to the tiers described for the pilot
597 library but with additional considerations:

598 Tier 1 (n=662 genes). For genes essential for growth in the K562 CRISPRi screen data
599 (p -value < 0.001 and $\gamma < -0.2$) (Horlbeck et al., 2016a), sgRNAs were ranked by their growth
600 phenotypes (calculated relative to the best-performing sgRNA targeting each gene per screen in
601 which the gene was a significant hit at FDR 0.05).

602 Tier 2 (n=4,033 genes): The ranking strategy used to generate the pilot library (dJR020)
603 included any gene identified as a significant hit in any previous CRISPRi screen for empirical
604 guide selection and as such did not control for the increased chance that a gene may score as a
605 false positive in a screen as the number of screens increases (the equivalent of multiple
606 comparisons). To control for such false positives, the 320 olfactory genes served as a negative
607 control set. None of the 320 olfactory genes were a significant hit [FDR 0.05 based on MAGeCK
608 RRA p -value (Li et al., 2014)] in greater than four previous CRISPRi screens. Therefore, as a

609 first cutoff, any gene that was identified as a significant hit in five or more previous CRISPRi
610 screens, regardless of the strength of the phenotype, was included in this tier.

611 This cutoff misses genes that score strongly, and as such are high-confidence hits, in a
612 small number of screens. To also include such genes, each gene that was a significant hit [FDR
613 0.05 based on MAGeCK RRA *p*-value (Li et al., 2014)] in one to four screens was assigned a
614 score based on the maximum absolute value discriminant score (calculated as the $-\log_{10}$ *p*-value
615 multiplied by the mean *z*-scored phenotype of the top three sgRNAs), summed across screens in
616 which the gene scored as a hit. As a comparison, this same score was calculated for olfactory
617 genes. Genes were included in this tier if the discriminant score was greater than a threshold
618 calculated from the olfactory gene scores for the same number of screens in which a gene was
619 identified as a hit.

620 For all genes included in this tier, sgRNAs were ranked by the average of phenotypes
621 across screens in which the gene was identified as a hit. Only sgRNAs that were identified as a
622 hit at FDR<0.01 in at least one screen were ranked. sgRNA phenotypes were calculated relative
623 to the best performing sgRNA targeting each gene per screen in which the gene was a significant
624 hit at FDR 0.05.

625 Tier 3 (n=14,493 genes): For all other genes, sgRNAs were ranked by the regression
626 scores in hCRISPRi v2.1 (Horlbeck et al., 2016a).

627 Using this ranking scheme, we selected the first and second ranked sgRNAs for a dual-
628 sgRNA/single-element-per-gene sublibrary (hCRISPRi_dual_1_2), the third and fourth ranked
629 sgRNAs for a second dual-sgRNA/single-element-per-gene sublibrary (hCRISPRi_dual_3_4),
630 and the fifth and sixth ranked sgRNAs for a final dual-sgRNA/single-element-per-gene
631 sublibrary (hCRISPRi_dual_5_6). Each library also contains a set of non-targeting control dual
632 sgRNAs representing 5% of the total library elements. A list of sgRNA targeting sequences for
633 all libraries is available in Table S3.

634 Integration barcodes (IBCs) were incorporated between the tandem sgRNA cassettes in
635 the dual-sgRNA library in four steps. First, a library of 215 8-nucleotide IBCs were designed
636 with a Hamming distance ≥ 4 and between 25-75% GC content (Table S4). Second, the library of
637 IBCs were cloned into pJR98 in an arrayed format. pJR98 was digested by AscI and ssDNA
638 oligo donors of the sequence 5' CTCTTCCTGCCCGACCTTGGGG – reverse complement IBC
639 – CAGCGCCATAGCTGAGTGTAGATTCGAGC – 3' were cloned into the vector using

640 NEBuilder HiFI DNA Assembly Master Mix (NEB). Third, the library of cloned IBCs were
641 Sanger verified and pooled at a equimolar ratio for all barcodes. Fourth, the library was cloned
642 into the dual-sgRNA library by BsmBI-digestion and ligation. Sequencing was performed on a
643 NovaSeq 6000 (Illumina) using a 19 bp Read 1, 19 bp Read 2, 8 bp Index Read 1, and 8 bp Index
644 Read 2 with custom sequencing primers as described in Supplementary Note 2. Demultiplexing
645 on only the i5 index using the i7 index (IBC) as a read was performed as detailed:
646 <https://gist.github.com/sumeetg23/a064a36801d2763e94da2e191699fb9f>.

647

648 *Perturb-seq comparison of dual sgRNA libraries versus Dolcetto*

649 Direct capture Perturb-seq (Replogle et al., 2020) was used to directly compare the knockdown
650 produced by the dual-sgRNA libraries versus the Dolcetto Set A CRISPRi library. N=128 genes
651 were randomly selected from the 4,000 most highly-expressed genes in K562 cells based on
652 RNA-seq (<https://www.encodeproject.org/experiments/ENCSR000AEL/>). Two parallel libraries
653 were cloned: a library containing the three dual-sgRNA elements targeting each gene and a
654 library containing the three Dolcetto Set A guides targeting each gene, plus non-targeting control
655 guides. For Dolcetto sgRNAs, the 5' base was replaced with a G to enable expression from the
656 U6 promoter. The Dolcetto single-sgRNA library was cloned as described above into pJR101
657 guide expression vector containing a Perturb-seq capture sequence in stem loop 2. The dual-
658 sgRNA library cloned as described above into pJR101 with a pJR98 insert cassette containing a
659 Perturb-seq capture sequence in stem loop 2 of guide B. After library verification by sequencing,
660 lentivirus was prepared in HEK293T as described above.

661 For Perturb-seq, CRISPRi K562 cells expressing dCas9-KOX1 KRAB (Gilbert et al.,
662 2014) were spinfected ($1000 \times g$) with polybrene (8 $\mu\text{g/ml}$) with lentivirus from both libraries in
663 parallel. Throughout the screen, cells were maintained at a density between 250,000 – 1,000,000
664 cells per ml and $1000\times$ coverage per library element. On day 3 post-transduction, an infection rate
665 of 5% was measured for both screens, and infected cells were sorted by FACS (BD FACS Aria).
666 On day 7 post-transduction, cells were prepared for single-cell RNA-sequencing as detailed in the
667 10x Genomics Single Cell Protocols Cell Preparation Guide (10x Genomics, CG00053 Rev C)
668 and separated into droplet emulsions using the Chromium Controller (10x Genomics) with
669 Chromium Single-Cell 3' Gel Beads v3.1 (10x Genomics, PN-1000121 and PN-1000120) across
670 12 lanes/gemgroups with the goal of recovering $\sim 15,000$ cells per GEM group before filtering.

671 Sequencing libraries were prepared following the 10x Genomics Chromium Single Cell 3' Reagent
672 Kits User Guide (v3.1 Chemistry) with Feature Barcoding technology for CRISPR Screening
673 (CG000205; Rev C). Libraries were sequenced on a NovaSeq 6000 (Illumina) according to the
674 10x Genomics User Guide.

675 After sequencing, mRNA and sgRNA counts were obtained from Cell Ranger 4.0.0
676 software (10x Genomics). To assign guides to cells, we used a Poisson-Gaussian mixture model
677 as previously described (Replogle et al., 2020). Only cells bearing a single Dolcetto sgRNA or a
678 single dual-sgRNA guide B sgRNA were used for downstream calculation of CRISPRi efficacy.
679 For each guide, the on-target knockdown was calculated as the fraction of mRNA remaining (target
680 gene expression in targeting cells relative to cells bearing non-targeting control guides).

681

682 *Design and cloning of constructs for CRISPRi effector expression*

683 All CRISPRi effectors were cloned into a lentiviral backbone containing a ubiquitous chromatin
684 opening element and a spleen focus forming virus (SFFV) promoter (pMH0001, Addgene #
685 85969). Briefly, dCas9, effector domains, linker domains, and GFP were PCR amplified and
686 inserted into backbone linearized by digest with MluI and NotI using Gibson assembly
687 (NEBuilder HiFi DNA Assembly Master Mix, NEB). P2A sequences were incorporated into
688 primer overhangs. The following additional considerations were incorporated into the final
689 construct designs:

- 690 1) For KRAB from Kox1, the KRAB(KOX1) domain from dCas9-BFP-KRAB (Addgene #
691 46911) was fused to the C-terminus of dCas9, because C-terminal fusions of
692 KRAB(KOX1) have historically produced the highest activity, linked by an 80-amino
693 acid linker (XTEN80). XTEN80-KRAB(KOX1) was synthesized as a gBlock (IDT). We
694 chose XTEN80 because we previously found that inclusion of a linker increases activity
695 and the original dCas9-BFP-KRAB(KOX1) construct (Gilbert et al., 2013) underwent
696 proteolytic cleavage between dCas9 and KRAB(KOX1) in some cell types, giving rise to
697 free dCas9, a dominant negative for CRISPRi. The final construct is dCas9-XTEN80-
698 KRAB(KOX1) or dCas9-Kox1 for short.
- 699 2) KRAB(ZIM3) was fused to the N-terminus of dCas9 with a 6-amino acid GS linker,
700 which had produced the highest activity in a previous report, including when compared to
701 C-terminal fusions (Alerasool et al., 2020). KRAB(ZIM3) was PCR-amplified from

702 pLX303-ZIM3-KRAB-dCas9 (Addgene # 154472). The final construct is KRAB(ZIM3)-
703 dCas9 or Zim3-dCas9 for short. Note that this construct contains an additional nuclear
704 localization signal between Zim3 and dCas9.

705 3) For SID4x, SID4x was fused to the N-terminus of dCas9-XTEN80-KRAB(Kox1),
706 because SID4x had previously only been evaluated for CRISPRi in the context of a dual
707 fusion (Carleton et al., 2017). A shorter 16-aa linker (XTEN16) was included between
708 SID4x and dCas9, which has been a sufficient linker length at the N-terminus in the past.
709 SID4x was amplified from a construct generously donated by the Aifantis lab (New York
710 University). The final construct is SID4x-XTEN16-dCas9-XTEN80-KRAB(KOX1) or
711 SID-dCas9-Kox1 for short.

712 4) For MeCP2, the previously reported dCas9-KRAB(Kox1)-MeCP2 construct (Addgene #
713 110821; Yeo et al., 2018) was PCR-amplified and transferred into the common backbone,
714 giving rise to dCas9-Kox1-MeCP2. Note that this construct contains no linker between
715 dCas9 and KRAB(Kox1), such that the KRAB(Kox1) domain may be largely inactive,
716 and that the dCas9 uses different codons. We separately also generated a construct in
717 which we fused MeCP2 to the C-terminus of the dCas9-XTEN80-KRAB(KOX1)
718 construct. We observed similar growth defects and non-specific effects on the
719 transcriptome using this construct.

720 Additional constructs with expression driven by a EF1 α promoter were generated by performing
721 analogous assemblies in the pMH0006 backbone (Addgene # 135448). Constructs with
722 expression driven by CMV or EFS promoters were generated by replacing the SFFV promoter in
723 existing constructs. Constructs in which effector expression is marked with BFP, mCherry, or
724 hygromycin resistance were generated by assembling with PCR products containing the desired
725 markers. Constructs in which expression of the fluorescent protein is linked by an internal
726 ribosome entry site (IRES) from encephalomyocarditis virus (EMCV) were generated by
727 incorporating a PCR fragment generated from pHR-TRE3G-TUBB-IRES-mCherry (Jost et al.,
728 2017) instead of the P2A site. Constructs in which EGFP is flanked by loxP sites were generated
729 by PCR-amplifying EGFP with primers containing loxP 2272 sequences
730 (ATAACTTCGTATAAAaGTATcCTATACGAAGTTAT). The amplicon was inserted by Gibson
731 Assembly into pJB069 or pJB109 linearized by digestion with NotI and AsiSI. Finally,
732 constructs in which the fluorescent proteins are constitutively linked to dCas9 were generated by

733 omitting the P2A sequence from primer overhangs. A full list of generated constructs is included
734 in Table S6. All constructs have been deposited to Addgene.

735

736 *Evaluation of effects of CRISPRi effectors on growth and transcription*

737 K562 cell lines stably expressing CRISPRi effectors from an SFFV promoter linked to GFP via
738 P2A were generated by lentiviral transduction and FACS. Each effector expression construct was
739 transduced in triplicate in parallel with all other constructs. 100,000 GFP-positive cells per
740 replicate were isolated by FACS on a Sony SH800S Cell Sorter 5 d after transduction and
741 allowed to recover.

742 To generate RNA-seq libraries of cells expressing each effector, 1×10^6 cells were
743 harvested for each sample 6 d after FACS by centrifugation at $300 \times g$ for 5 min and flash frozen
744 in a dry ice and ethanol bath. RNA was extracted using the Direct-zol RNA Miniprep kit (Zymo
745 Research) and quantified using the Qubit RNA BR Assay Kit (Life Technologies). RNA-seq
746 libraries were prepared by the Whitehead Genome Technology Core facility using the Roche
747 Diagnostics KAPA mRNA HyperPrep Kit. Paired-end 100 sequencing was performed on a
748 NovaSeq (Illumina).

749 To evaluate growth of CRISPRi effector-expressing cells, a reference population of K562
750 cells stably expressing mCherry was generated by lentiviral transduction of pU6-sgRNA
751 EF1Alpha-puro-T2A-mCherry (a gift from Gregory Ow and Eric Collisson, UCSF) and FACS.
752 This was conducted in parallel with the generation of CRISPRi effector-expressing cells. 7 days
753 after sorting, $\sim 125,000$ cells per GFP-sorted population (different CRISPRi effectors) were
754 mixed with $\sim 125,000$ mCherry-sorted cells (reference population). The ratio of mCherry-positive
755 to mCherry-negative cells was read out immediately after mixing and periodically for the next 19
756 days by flow cytometry on an Attune NxT (ThermoFisher).

757

758 *RNA-seq data analysis*

759 Sequencing reads were aligned strand-specifically to the human genome (GRCh38) and then
760 aggregated by gene using only reads uniquely mapped to the reverse strand using the spliced
761 read aligner STAR (Dobin et al., 2013), version 2.7.9, against an index containing features from
762 Ensembl release 98 / GENCODE v32 (downloaded from 10x Genomics reference 2020-A).

763 Replicate sample 2 for cells expressing dCas9-Kox1 had substantially fewer reads than expected

764 and was excluded from analysis. For clustering analysis, transcript counts were normalized to
765 transcripts per million for each sample, filtered for the 2000 most highly expressed genes on
766 average, and clustered using the Ward variance minimization algorithm implemented in *scipy*
767 version 1.6.2. Differential expression analysis was carried out on gene counts using DESeq2
768 (Love et al., 2014). For Figure 2E, transcript counts were not filtered. The trends for numbers of
769 differentially expressed genes were equivalent when only including genes with an average count
770 > 2 across all samples.

771

772 *Selection and cloning of individual sgRNAs*

773 Strong sgRNAs against essential genes or cell surface markers were selected from the
774 hCRISPRi-v2 library (Horlbeck et al., 2016a; Nuñez et al., 2021). Intermediate-activity sgRNAs
775 were selected either from the hCRISPRi-v2 library or by incorporating defined mismatches in
776 strong sgRNAs (Jost et al., 2020). All sgRNA sequences used for individual evaluation are listed
777 in Table S6.

778 Individual sgRNA expression constructs were cloned as described previously (Gilbert et
779 al., 2014). Briefly, two complementary oligonucleotides (IDT), containing the sgRNA targeting
780 region as well as overhangs matching those left by restriction digest of the vector with BstXI and
781 BlnI, were annealed and ligated into pCRISPRi-v2 [pU6-sgRNA EF1Alpha-puro-T2A-BFP
782 with two SbfI sites flanking the sgRNA expression cassette, Addgene #84832 (Horlbeck et al.,
783 2016a)] or pU6-sgRNA EF1Alpha-puro-T2A-mCherry [a gift from Gregory Ow and Eric
784 Collisson, UCSF, (Jost et al., 2020)] digested with BstXI (NEB or Thermo Fisher Scientific) and
785 BlnI (NEB) or Bpu1102I (Thermo Fisher Scientific). The ligation product was transformed into
786 Stellar chemically competent *E. coli* cells (Takara Bio) and plasmid was prepared following
787 standard protocols. The resulting sgRNA expression vectors were individually packaged into
788 lentivirus as described above.

789

790 *Evaluation of individual sgRNA phenotypes*

791 Effects of sgRNAs targeting essential genes on cell growth were measured in internally
792 controlled growth assays by transducing cells with mCherry-marked sgRNA expression
793 constructs at MOI < 0.5 (15 – 40% infected cells) and measuring the fraction of sgRNA-
794 expressing cells 3-12 days after transduction as mCherry-positive cells by flow cytometry on an

795 Attune NxT (ThermoFisher). All experiments were performed in duplicates from the infection
796 step.

797 Effects of sgRNAs on expression levels of cell surface proteins were measured by flow
798 cytometry. K562 or Jurkat cell lines expressing CRISPRi effectors of interest were infected with
799 lentivirus containing sgRNA expression vectors by centrifugation at $1000 \times g$ for 1 h in 24-well
800 plates in the presence of 8 $\mu\text{g}/\text{mL}$ polybrene (Sigma-Aldrich). RPE1, HepG2, HuTu-80, and
801 HT29 cell lines expressing Zim3-dCas9 were infected with lentivirus containing sgRNA
802 expression vectors for 24 h in the presence of 8 $\mu\text{g}/\text{mL}$ polybrene. 6-14 d after transduction, cells
803 were harvested by centrifugation (suspension cells) or trypsin-free detachment (adherent cells;
804 mechanical detachment or EDTA), washed once in flow cytometry buffer (PBS with 5% (v/v)
805 FBS), and stained at room temperature for 15-30 min with APC-conjugated antibodies targeting
806 CD55 (clone JS11, BioLegend 311311), CD81 (clone 5A6, Biolegend 349509), CD151 (clone
807 50-6, BioLegend 350405), CD29 (clone TS2/16, Biolegend 303007), or B2M (clone 2M2,
808 Biolegend 316312) diluted 1:100 in flow cytometry buffer. After staining, cells were washed
809 twice in 200 μL flow cytometry buffer and resuspended in flow cytometry buffer for
810 measurement on an Attune NxT (ThermoFisher), LSR-II (BD Biosciences) or Symphony A3
811 (BD Biosciences).

812 Optimal dilutions for each antibody were determined by testing 1:20, 1:100, and 1:500
813 antibody titrations on K562 cells with epitope-targeting or non-targeting sgRNAs and choosing
814 the titration with the maximum signal difference.

815 Flow cytometry data were analyzed using FlowCytometryTools 0.5.0
816 (<https://eyurtsev.github.io/FlowCytometryTools/>) and python 3.8. Briefly, the data were gated
817 for cells (FSC-A versus SSC-A), FSC singlets (FSC-W versus FSC-H for data recorded on an
818 Attune NxT and FSC-W versus FSC-A for data recorded on an LSR-II), SSC singlets (SSC-W
819 versus SSC-H for data recorded on an Attune NxT and SSC-W versus SSC-A for data recorded
820 on an LSR-II), and sgRNA-expressing cells (BFP- or mCherry-positive, depending on the
821 experiment). Background APC fluorescence intensity from unstained cells or cells stained with
822 an APC-conjugated Mouse IgG1, κ isotype control (BioLegend clone MOPC-21) was subtracted
823 to correct for background fluorescence. Knockdown was quantified using median background-
824 corrected APC fluorescence intensity in cells expressing a targeting sgRNA relative to intensity
825 in cells expressing a non-targeting control sgRNA, with the exception of the Jurkat and RPE1

826 experiments, for which knockdown was quantified using median background-corrected APC
827 fluorescence intensity in cells expressing a targeting sgRNA relative to intensity in cells not
828 expressing an sgRNA in the same well.
829

830 References

- 831
832
833 Adamson B, Norman TM, Jost M, Cho MY, Nuñez JK, Chen Y, Villalta JE, Gilbert LA,
834 Horlbeck MA, Hein MY, Pak RA, Gray AN, Gross CA, Dixit A, Parnas O, Regev A,
835 Weissman JS. 2016. A Multiplexed Single-Cell CRISPR Screening Platform Enables
836 Systematic Dissection of the Unfolded Protein Response. *Cell* 167:1867-1882.e21.
837 doi:10.1016/j.cell.2016.11.048
- 838 Adamson B, Norman TM, Jost M, Weissman JS. 2018. Approaches to maximize sgRNA-
839 barcode coupling in Perturb-seq screens. *Biorxiv* 298349. doi:10.1101/298349
- 840 Alerasool N, Segal D, Lee H, Taipale M. 2020. An efficient KRAB domain for CRISPRi
841 applications in human cells. *Nat Methods* 17:1093–1096. doi:10.1038/s41592-020-0966-x
- 842 Behan FM, Iorio F, Picco G, Gonçalves E, Beaver CM, Migliardi G, Santos R, Rao Y, Sassi F,
843 Pinnelli M, Ansari R, Harper S, Jackson DA, McRae R, Pooley R, Wilkinson P, Meer D van
844 der, Dow D, Buser-Doepner C, Bertotti A, Trusolino L, Stronach EA, Saez-Rodriguez J, Yusa
845 K, Garnett MJ. 2019. Prioritization of cancer therapeutic targets using CRISPR–Cas9 screens.
846 *Nature* 568:511–516. doi:10.1038/s41586-019-1103-9
- 847 Bock C, Datlinger P, Chardon F, Coelho MA, Dong MB, Lawson KA, Lu T, Maroc L, Norman
848 TM, Song B, Stanley G, Chen S, Garnett M, Li W, Moffat J, Qi LS, Shapiro RS, Shendure J,
849 Weissman JS, Zhuang X. 2022. High-content CRISPR screening. *Nat Rev Methods Primers*
850 2:8. doi:10.1038/s43586-021-00093-4
- 851 Bosch B, DeJesus MA, Poulton NC, Zhang W, Engelhart CA, Zaveri A, Lavalette S, Ruecker N,
852 Trujillo C, Wallach JB, Li S, Ehrt S, Chait BT, Schnappinger D, Rock JM. 2021. Genome-
853 wide gene expression tuning reveals diverse vulnerabilities of *M. tuberculosis*. *Cell* 184:4579-
854 4592.e24. doi:10.1016/j.cell.2021.06.033
- 855 Bowden AR, Morales-Juarez DA, Sczaniecka-Clift M, Agudo MM, Lukashchuk N, Thomas JC,
856 Jackson SP. 2020. Parallel CRISPR-Cas9 screens clarify impacts of p53 on screen
857 performance. *Elife* 9:e55325. doi:10.7554/elife.55325
- 858 Carleton JB, Berrett KC, Gertz J. 2017. Multiplex Enhancer Interference Reveals Collaborative
859 Control of Gene Regulation by Estrogen Receptor α -Bound Enhancers. *Cell Syst* 5:333-
860 344.e5. doi:10.1016/j.cels.2017.08.011
- 861 Coukos R, Yao D, Sanchez MI, Strand ET, Olive ME, Udeshi ND, Weissman JS, Carr SA,
862 Bassik MC, Ting AY. 2021. An engineered transcriptional reporter of protein localization
863 identifies regulators of mitochondrial and ER membrane protein trafficking in high-
864 throughput CRISPRi screens. *Elife* 10:e69142. doi:10.7554/elife.69142
- 865 Dobin A, Davis CA, Schlesinger F, Drenkow J, Zaleski C, Jha S, Batut P, Chaisson M, Gingeras
866 TR. 2013. STAR: ultrafast universal RNA-seq aligner. *Bioinformatics* 29:15–21.
867 doi:10.1093/bioinformatics/bts635
- 868 Doench JG. 2018. Am I ready for CRISPR? A user’s guide to genetic screens. *Nat Rev Genet*
869 19:67–80. doi:10.1038/nrg.2017.97
- 870 Dong F, Xie K, Chen Y, Yang Y, Mao Y. 2017. Polycistronic tRNA and CRISPR guide-RNA
871 enables highly efficient multiplexed genome engineering in human cells. *Biochem Bioph Res*
872 *Co* 482:889–895. doi:10.1016/j.bbrc.2016.11.129
- 873 Dräger NM, Sattler SM, Huang CT-L, Teter OM, Leng K, Hashemi SH, Hong J, Aviles G,
874 Clelland CD, Zhan L, Udeochu JC, Kodama L, Singleton AB, Nalls MA, Ichida J, Ward ME,
875 Faghri F, Gan L, Kampmann M. 2022. A CRISPRi/a platform in iPSC-derived microglia

- 876 uncovers regulators of disease states. *Biorxiv* 2021.06.16.448639.
877 doi:10.1101/2021.06.16.448639
- 878 Du D, Roguev A, Gordon DE, Chen M, Chen S-H, Shales M, Shen JP, Ideker T, Mali P, Qi LS,
879 Krogan NJ. 2017. Genetic interaction mapping in mammalian cells using CRISPR
880 interference. *Nat Methods* 14:577–580. doi:10.1038/nmeth.4286
- 881 Ecco G, Imbeault M, Trono D. 2017. KRAB zinc finger proteins. *Development* 144:2719–2729.
882 doi:10.1242/dev.132605
- 883 Feldman D, Singh A, Garrity AJ, Blainey PC. 2018. Lentiviral co-packaging mitigates the effects
884 of intermolecular recombination and multiple integrations in pooled genetic screens. *Biorxiv*
885 262121. doi:10.1101/262121
- 886 Fulco CP, Munschauer M, Anyoha R, Munson G, Grossman SR, Perez EM, Kane M, Cleary B,
887 Lander ES, Engreitz JM. 2016. Systematic mapping of functional enhancer–promoter
888 connections with CRISPR interference. *Science* 354:769–773. doi:10.1126/science.aag2445
- 889 Fulco CP, Nasser J, Jones TR, Munson G, Bergman DT, Subramanian V, Grossman SR, Anyoha
890 R, Doughty BR, Patwardhan TA, Nguyen TH, Kane M, Perez EM, Durand NC, Lareau CA,
891 Stamenova EK, Aiden EL, Lander ES, Engreitz JM. 2019. Activity-by-Contact model of
892 enhancer-promoter regulation from thousands of CRISPR perturbations. *Nat Genet* 51:1664–
893 1669. doi:10.1038/s41588-019-0538-0
- 894 Gasperini M, Hill AJ, McFaline-Figueroa JL, Martin B, Kim S, Zhang MD, Jackson D, Leith A,
895 Schreiber J, Noble WS, Trapnell C, Ahituv N, Shendure J. 2019. A Genome-wide Framework
896 for Mapping Gene Regulation via Cellular Genetic Screens. *Cell* 176:377-390.e19.
897 doi:10.1016/j.cell.2018.11.029
- 898 Gilbert LA, Horlbeck MA, Adamson B, Villalta JE, Chen Y, Whitehead EH, Guimaraes C,
899 Panning B, Ploegh HL, Bassik MC, Qi LS, Kampmann M, Weissman JS. 2014. Genome-
900 Scale CRISPR-Mediated Control of Gene Repression and Activation. *Cell* 159:647–661.
901 doi:10.1016/j.cell.2014.09.029
- 902 Gilbert LA, Larson MH, Morsut L, Liu Z, Brar GA, Torres SE, Stern-Ginossar N, Brandman O,
903 Whitehead EH, Doudna JA, Lim WA, Weissman JS, Qi LS. 2013. CRISPR-Mediated
904 Modular RNA-Guided Regulation of Transcription in Eukaryotes. *Cell* 154:442–451.
905 doi:10.1016/j.cell.2013.06.044
- 906 Haapaniemi E, Botla S, Persson J, Schmierer B, Taipale J. 2018. CRISPR–Cas9 genome editing
907 induces a p53-mediated DNA damage response. *Nat Med* 24:927–930. doi:10.1038/s41591-
908 018-0049-z
- 909 Haswell JR, Mattioli K, Gerhardinger C, Maass PG, Foster DJ, Peinado P, Wang X, Medina PP,
910 Rinn JL, Slack FJ. 2021. Genome-wide CRISPR interference screen identifies long non-
911 coding RNA loci required for differentiation and pluripotency. *Plos One* 16:e0252848.
912 doi:10.1371/journal.pone.0252848
- 913 Hawkins JS, Silvis MR, Koo B-M, Peters JM, Osadnik H, Jost M, Hearne CC, Weissman JS,
914 Todor H, Gross CA. 2020. Mismatch-CRISPRi Reveals the Co-varying Expression-Fitness
915 Relationships of Essential Genes in Escherichia coli and Bacillus subtilis. *Cell Syst* 11:523-
916 535.e9. doi:10.1016/j.cels.2020.09.009
- 917 Hill AJ, McFaline-Figueroa JL, Starita LM, Gasperini MJ, Matreyek KA, Packer J, Jackson D,
918 Shendure J, Trapnell C. 2018. On the design of CRISPR-based single-cell molecular screens.
919 *Nat Methods* 15:271–274. doi:10.1038/nmeth.4604

- 920 Horlbeck MA, Gilbert LA, Villalta JE, Adamson B, Pak RA, Chen Y, Fields AP, Park CY, Corn
921 JE, Kampmann M, Weissman JS. 2016a. Compact and highly active next-generation libraries
922 for CRISPR-mediated gene repression and activation. *Elife* 5:e19760. doi:10.7554/elife.19760
- 923 Horlbeck MA, Witkowsky LB, Guglielmi B, Replogle JM, Gilbert LA, Villalta JE, Torigoe SE,
924 Tjian R, Weissman JS. 2016b. Nucleosomes impede Cas9 access to DNA in vivo and in vitro.
925 *Elife* 5:e12677. doi:10.7554/elife.12677
- 926 Horlbeck MA, Xu A, Wang M, Bennett NK, Park CY, Bogdanoff D, Adamson B, Chow ED,
927 Kampmann M, Peterson TR, Nakamura K, Fischbach MA, Weissman JS, Gilbert LA. 2018.
928 Mapping the Genetic Landscape of Human Cells. *Cell* 174:953-967.e22.
929 doi:10.1016/j.cell.2018.06.010
- 930 Ihry RJ, Worringer KA, Salick MR, Frias E, Ho D, Theriault K, Kommineni S, Chen J, Sondey
931 M, Ye C, Randhawa R, Kulkarni T, Yang Z, McAllister G, Russ C, Reece-Hoyes J, Forrester
932 W, Hoffman GR, Dolmetsch R, Kaykas A. 2018. p53 inhibits CRISPR–Cas9 engineering in
933 human pluripotent stem cells. *Nat Med* 24:939–946. doi:10.1038/s41591-018-0050-6
- 934 Jost M, Chen Y, Gilbert LA, Horlbeck MA, Krenning L, Menchon G, Rai A, Cho MY, Stern JJ,
935 Prota AE, Kampmann M, Akhmanova A, Steinmetz MO, Tanenbaum ME, Weissman JS.
936 2017. Combined CRISPRi/a-Based Chemical Genetic Screens Reveal that Rigosertib Is a
937 Microtubule-Destabilizing Agent. *Mol Cell* 68:210-223.e6. doi:10.1016/j.molcel.2017.09.012
- 938 Jost M, Santos DA, Saunders RA, Horlbeck MA, Hawkins JS, Scaria SM, Norman TM,
939 Hussmann JA, Liem CR, Gross CA, Weissman JS. 2020. Titrating gene expression using
940 libraries of systematically attenuated CRISPR guide RNAs. *Nat Biotechnol* 38:355–364.
941 doi:10.1038/s41587-019-0387-5
- 942 Kearns NA, Pham H, Tabak B, Genga RM, Silverstein NJ, Garber M, Maehr R. 2015. Functional
943 annotation of native enhancers with a Cas9 -histone demethylase fusion. *Nat Methods*
944 12:401–403. doi:10.1038/nmeth.3325
- 945 Klann TS, Black JB, Chellappan M, Safi A, Song L, Hilton IB, Crawford GE, Reddy TE,
946 Gersbach CA. 2017. CRISPR–Cas9 epigenome editing enables high-throughput screening for
947 functional regulatory elements in the human genome. *Nat Biotechnol* 35:561–568.
948 doi:10.1038/nbt.3853
- 949 Knapp DJHF, Michaels YS, Jamilly M, Ferry QRV, Barbosa H, Milne TA, Fulga TA. 2019.
950 Decoupling tRNA promoter and processing activities enables specific Pol-II Cas9 guide RNA
951 expression. *Nat Commun* 10:1490. doi:10.1038/s41467-019-09148-3
- 952 Kosicki M, Tomberg K, Bradley A. 2018. Repair of double-strand breaks induced by CRISPR–
953 Cas9 leads to large deletions and complex rearrangements. *Nat Biotechnol* 36:765–771.
954 doi:10.1038/nbt.4192
- 955 Leng K, Rose IVL, Kim H, Xia W, Romero-Fernandez W, Rooney B, Koontz M, Li E, Ao Y,
956 Wang S, Krawczyk M, TCW J, Goate A, Zhang Y, Ullian EM, Sofroniew MV, Fancy SPJ,
957 Schrag MS, Lippmann ES, Kampmann M. 2022. CRISPRi screens in human astrocytes
958 elucidate regulators of distinct inflammatory reactive states. *Biorxiv* 2021.08.23.457400.
959 doi:10.1101/2021.08.23.457400
- 960 Li W, Xu H, Xiao T, Cong L, Love MI, Zhang F, Irizarry RA, Liu JS, Brown M, Liu XS. 2014.
961 MAGeCK enables robust identification of essential genes from genome-scale CRISPR/Cas9
962 knockout screens. *Genome Biol* 15:554. doi:10.1186/s13059-014-0554-4
- 963 Liang JR, Lingeman E, Luong T, Ahmed S, Muhar M, Nguyen T, Olzmann JA, Corn JE. 2020.
964 A Genome-wide ER-phagy Screen Highlights Key Roles of Mitochondrial Metabolism and
965 ER-Resident UFMylation. *Cell* 180:1160-1177.e20. doi:10.1016/j.cell.2020.02.017

- 966 Liu SJ, Horlbeck MA, Cho SW, Birk HS, Malatesta M, He D, Attenello FJ, Villalta JE, Cho MY,
967 Chen Y, Mandegar MA, Olvera MP, Gilbert LA, Conklin BR, Chang HY, Weissman JS, Lim
968 DA. 2017. CRISPRi-based genome-scale identification of functional long noncoding RNA
969 loci in human cells. *Science* 355. doi:10.1126/science.aah7111
- 970 Love MI, Huber W, Anders S. 2014. Moderated estimation of fold change and dispersion for
971 RNA-seq data with DESeq2. *Genome Biol* 15:550. doi:10.1186/s13059-014-0550-8
- 972 Luteijn RD, Zaver SA, Gowen BG, Wyman S, Garelis N, Onia L, McWhirter SM, Katibah GE,
973 Corn JE, Woodward JJ, Raulet DH. 2019. SLC19A1 transports immunoreactive cyclic
974 dinucleotides. *Nature* 573:434–438. doi:10.1038/s41586-019-1553-0
- 975 Mandegar MA, Huebsch N, Frolov EB, Shin E, Truong A, Olvera MP, Chan AH, Miyaoka Y,
976 Holmes K, Spencer CI, Judge LM, Gordon DE, Eskildsen TV, Villalta JE, Horlbeck MA,
977 Gilbert LA, Krogan NJ, Sheikh SP, Weissman JS, Qi LS, So P-L, Conklin BR. 2016.
978 CRISPR Interference Efficiently Induces Specific and Reversible Gene Silencing in Human
979 iPSCs. *Cell Stem Cell* 18:541–553. doi:10.1016/j.stem.2016.01.022
- 980 Meyers RM, Bryan JG, McFarland JM, Weir BA, Sizemore AE, Xu H, Dharia NV, Montgomery
981 PG, Cowley GS, Pantel S, Goodale A, Lee Y, Ali LD, Jiang G, Lubonja R, Harrington WF,
982 Strickland M, Wu T, Hawes DC, Zhivich VA, Wyatt MR, Kalani Z, Chang JJ, Okamoto M,
983 Stegmaier K, Golub TR, Boehm JS, Vazquez F, Root DE, Hahn WC, Tsherniak A. 2017.
984 Computational correction of copy number effect improves specificity of CRISPR–Cas9
985 essentiality screens in cancer cells. *Nat Genet* 49:1779–1784. doi:10.1038/ng.3984
- 986 Michlits G, Hubmann M, Wu S-H, Vainorius G, Budusan E, Zhuk S, Burkard TR, Novatchkova
987 M, Aichinger M, Lu Y, Reece-Hoyes J, Nitsch R, Schramek D, Hoepfner D, Elling U. 2017.
988 CRISPR-UMI: single-cell lineage tracing of pooled CRISPR–Cas9 screens. *Nat Methods*
989 14:1191–1197. doi:10.1038/nmeth.4466
- 990 Morgens DW, Chan C, Kane AJ, Weir NR, Li A, Dubreuil MM, Tsui CK, Hess GT, Lavertu A,
991 Han K, Polyakov N, Zhou J, Handy EL, Alabi P, Dombroski A, Yao D, Altman RB, Sello JK,
992 Denic V, Bassik MC. 2019. Retro-2 protects cells from ricin toxicity by inhibiting ASNA1-
993 mediated ER targeting and insertion of tail-anchored proteins. *Elife* 8:e48434.
994 doi:10.7554/elife.48434
- 995 Nuñez JK, Chen J, Pommier GC, Cogan JZ, Replogle JM, Adriaens C, Ramadoss GN, Shi Q,
996 Hung KL, Samelson AJ, Pogson AN, Kim JYS, Chung A, Leonetti MD, Chang HY,
997 Kampmann M, Bernstein BE, Hovestadt V, Gilbert LA, Weissman JS. 2021. Genome-wide
998 programmable transcriptional memory by CRISPR-based epigenome editing. *Cell* 184:2503-
999 2519.e17. doi:10.1016/j.cell.2021.03.025
- 1000 Przybyla L, Gilbert LA. 2021. A new era in functional genomics screens. *Nat Rev Genet* 1–15.
1001 doi:10.1038/s41576-021-00409-w
- 1002 Raffener P, Hart JR, García-Caballero D, Bar-Peled L, Weinberg MS, Vogt PK. 2020. An
1003 MXD1-derived repressor peptide identifies noncoding mediators of MYC-driven cell
1004 proliferation. *Proc National Acad Sci* 117:6571–6579. doi:10.1073/pnas.1921786117
- 1005 Replogle JM, Norman TM, Xu A, Hussmann JA, Chen J, Cogan JZ, Meer EJ, Terry JM, Riordan
1006 DP, Srinivas N, Fiddes IT, Arthur JG, Alvarado LJ, Pfeiffer KA, Mikkelsen TS, Weissman
1007 JS, Adamson B. 2020. Combinatorial single-cell CRISPR screens by direct guide RNA
1008 capture and targeted sequencing. *Nat Biotechnol* 38:954–961. doi:10.1038/s41587-020-0470-
1009 y
- 1010 Replogle JM, Saunders RA, Pogson AN, Hussmann JA, Lenail A, Guna A, Mascibroda L,
1011 Wagner EJ, Adelman K, Lithwick-Yanai G, Iremadze N, Oberstrass F, Lipson D, Bonnar JL,

- 1012 Jost M, Norman TM, Weissman JS. 2022. Mapping information-rich genotype-phenotype
1013 landscapes with genome-scale Perturb-seq. *Cell*. doi:10.1016/j.cell.2022.05.013
- 1014 Sage C le, Lawo S, Panicker P, Scales TME, Rahman SA, Little AS, McCarthy NJ, Moore JD,
1015 Cross BCS. 2017. Dual direction CRISPR transcriptional regulation screening uncovers gene
1016 networks driving drug resistance. *Sci Rep-uk* 7:17693. doi:10.1038/s41598-017-18172-6
- 1017 Sanson KR, Hanna RE, Hegde M, Donovan KF, Strand C, Sullender ME, Vaimberg EW,
1018 Goodale A, Root DE, Piccioni F, Doench JG. 2018. Optimized libraries for CRISPR-Cas9
1019 genetic screens with multiple modalities. *Nat Commun* 9:5416. doi:10.1038/s41467-018-
1020 07901-8
- 1021 Schellenberger V, Wang C, Geething NC, Spink BJ, Campbell A, To W, Scholle MD, Yin Y,
1022 Yao Y, Bogin O, Cleland JL, Silverman J, Stemmer WPC. 2009. A recombinant polypeptide
1023 extends the in vivo half-life of peptides and proteins in a tunable manner. *Nat Biotechnol*
1024 27:1186–1190. doi:10.1038/nbt.1588
- 1025 Schmidt R, Steinhart Z, Layeghi M, Freimer JW, Bueno R, Nguyen VQ, Blaeschke F, Ye CJ,
1026 Marson A. 2022. CRISPR activation and interference screens decode stimulation responses in
1027 primary human T cells. *Sci New York N Y* 375:eabj4008. doi:10.1126/science.abj4008
- 1028 Semesta KM, Tian R, Kampmann M, Zastrow M von, Tsvetanova NG. 2020. A high-throughput
1029 CRISPR interference screen for dissecting functional regulators of GPCR/cAMP signaling.
1030 *Plos Genet* 16:e1009103. doi:10.1371/journal.pgen.1009103
- 1031 Smits AH, Ziebell F, Joberty G, Zinn N, Mueller WF, Clauder-Münster S, Eberhard D, Savitski
1032 MF, Grandi P, Jakob P, Michon A-M, Sun H, Tessmer K, Bürckstümmer T, Bantscheff M,
1033 Steinmetz LM, Drewes G, Huber W. 2019. Biological plasticity rescues target activity in
1034 CRISPR knock outs. *Nat Methods* 16:1087–1093. doi:10.1038/s41592-019-0614-5
- 1035 Thakore PI, D’Ippolito AM, Song L, Safi A, Shivakumar NK, Kabadi AM, Reddy TE, Crawford
1036 GE, Gersbach CA. 2015. Highly specific epigenome editing by CRISPR-Cas9 repressors for
1037 silencing of distal regulatory elements. *Nat Methods* 12:1143–1149. doi:10.1038/nmeth.3630
- 1038 Tian R, Abarientos A, Hong J, Hashemi SH, Yan R, Dräger N, Leng K, Nalls MA, Singleton
1039 AB, Xu K, Faghri F, Kampmann M. 2021. Genome-wide CRISPRi/a screens in human
1040 neurons link lysosomal failure to ferroptosis. *Nat Neurosci* 24:1020–1034.
1041 doi:10.1038/s41593-021-00862-0
- 1042 Tian R, Gachechiladze MA, Ludwig CH, Laurie MT, Hong JY, Nathaniel D, Prabhu AV,
1043 Fernandopulle MS, Patel R, Abshari M, Ward ME, Kampmann M. 2019. CRISPR
1044 Interference-Based Platform for Multimodal Genetic Screens in Human iPSC-Derived
1045 Neurons. *Neuron* 104:239-255.e12. doi:10.1016/j.neuron.2019.07.014
- 1046 Tsherniak A, Vazquez F, Montgomery PG, Weir BA, Kryukov G, Cowley GS, Gill S,
1047 Harrington WF, Pantel S, Krill-Burger JM, Meyers RM, Ali L, Goodale A, Lee Y, Jiang G,
1048 Hsiao J, Gerath WFJ, Howell S, Merkel E, Ghandi M, Garraway LA, Root DE, Golub TR,
1049 Boehm JS, Hahn WC. 2017. Defining a Cancer Dependency Map. *Cell* 170:564-576.e16.
1050 doi:10.1016/j.cell.2017.06.010
- 1051 Xie S, Cooley A, Armendariz D, Zhou P, Hon GC. 2018. Frequent sgRNA-barcode
1052 recombination in single-cell perturbation assays. *Plos One* 13:e0198635.
1053 doi:10.1371/journal.pone.0198635
- 1054 Yeo NC, Chavez A, Lance-Byrne A, Chan Y, Menn D, Milanova D, Kuo C-C, Guo X, Sharma
1055 S, Tung A, Cecchi RJ, Tuttle M, Pradhan S, Lim ET, Davidsohn N, Ebrahimkhani MR,
1056 Collins JJ, Lewis NE, Kiani S, Church GM. 2018. An enhanced CRISPR repressor for

1057 targeted mammalian gene regulation. *Nat Methods* 15:611–616. doi:10.1038/s41592-018-
1058 0048-5
1059 Yin JA, Frick L, Scheidmann MC, Trevisan C, Dhingra A, Spinelli A, Wu Y, Yao L, Vena DL,
1060 De Cecco E, Ging K, Liu T, Täger J, Rodriguez S, Guo J, Berry S, Losa M, Hornemann S,
1061 Kampmann M, Pelkmans L, Hoepfner D, Heutink P, Aguzzi A. 2022. Robust and Versatile
1062 Arrayed Libraries for Human Genome-Wide CRISPR Activation, Deletion and Silencing.
1063 *bioRxiv*. doi:10.1101/2022.05.25.493370
1064 Zhu S, Cao Z, Liu Z, He Y, Wang Y, Yuan P, Li W, Tian F, Bao Y, Wei W. 2019. Guide RNAs
1065 with embedded barcodes boost CRISPR-pooled screens. *Genome Biol* 20:20.
1066 doi:10.1186/s13059-019-1628-0
1067
1068
1069
1070

1071 **Figures and Figure Legends**

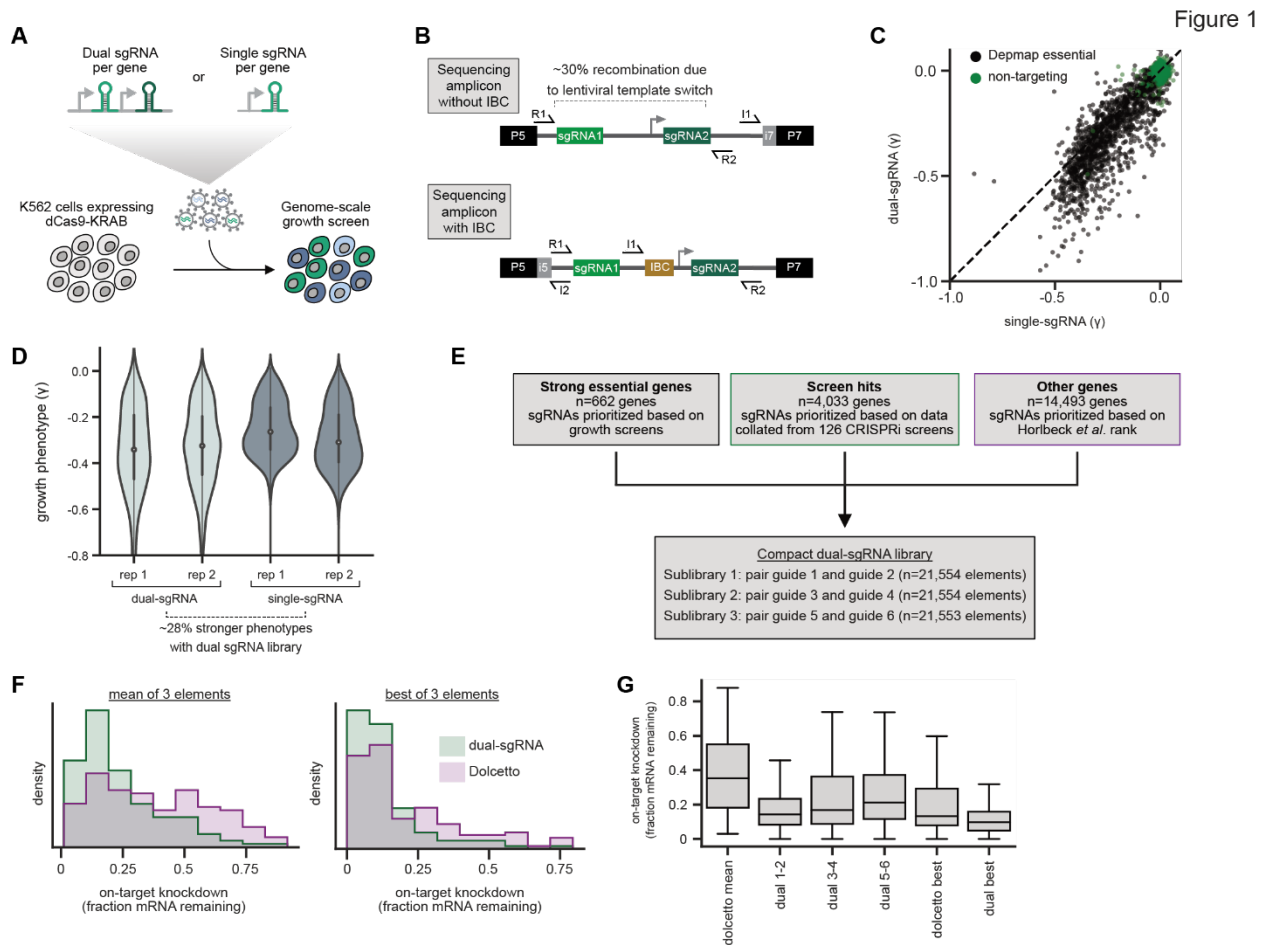


Figure 1

1072

1073 **Figure 1. Design and validation of ultra-compact dual-sgRNA CRISPRi libraries.**

1074 a. Schematic of growth screen used to compare single- and dual-sgRNA libraries.

1075 b. Schematic of dual-sgRNA library sequencing strategies.

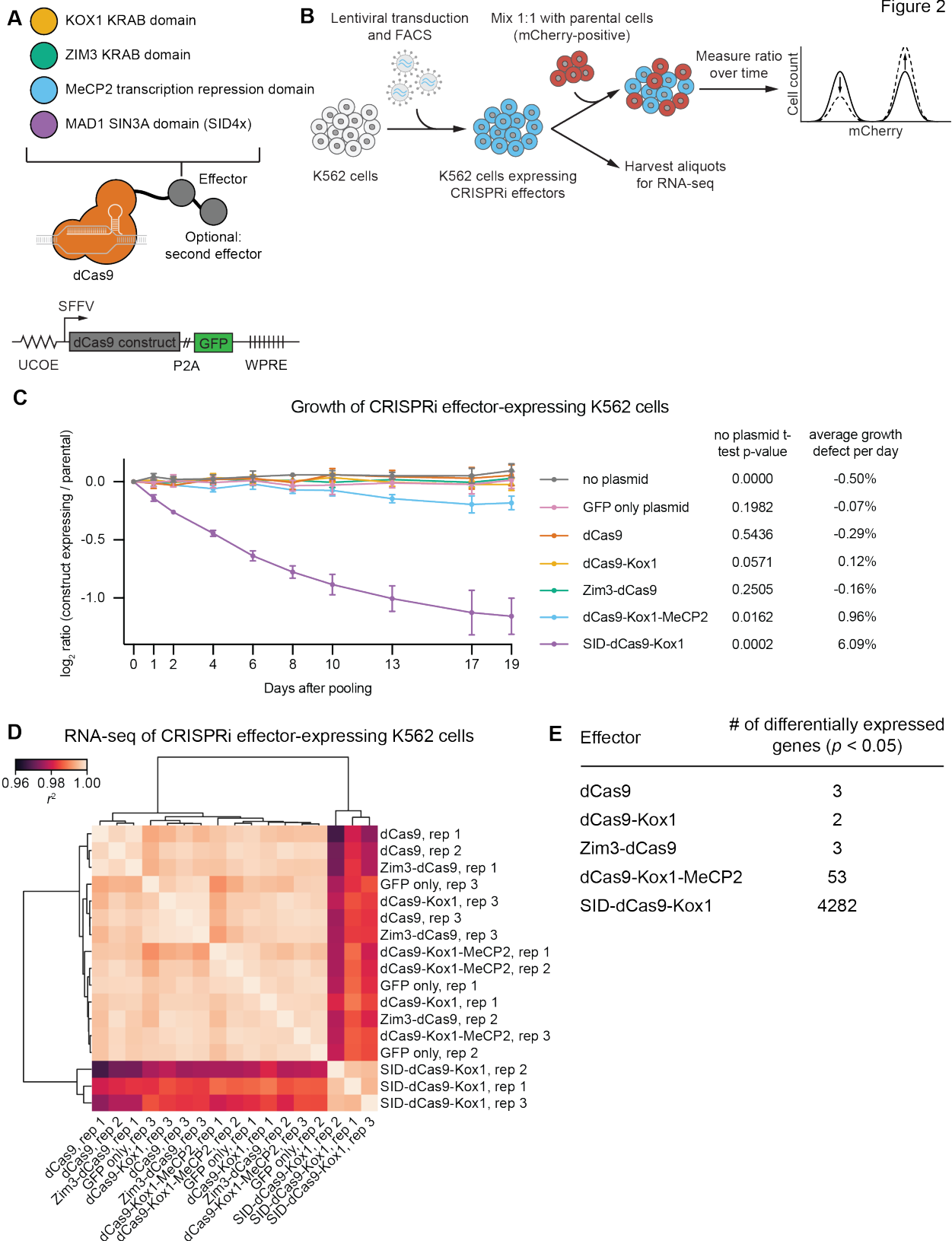
1076 c. Comparison of growth phenotypes for DepMap essential genes between single- and dual-
1077 sgRNA libraries. Sequencing libraries were prepared using the strategy labeled “Sequencing
1078 amplicon without IBC” in panel b. Growth phenotypes are reported as γ (\log_2 fold-enrichment of
1079 T_{final} over T_0 , per doubling) and well-correlated between libraries ($r = 0.91$).

1080 d. Comparison of growth phenotypes for DepMap essential genes between single- and dual-
1081 sgRNA libraries.

1082 e. Design of final dual-sgRNA library.

1083 f. Comparison of target gene knockdown by dual-sgRNA library versus Dolcetto. Target gene
1084 knockdown was measured by single-cell RNA-sequencing (Perturb-seq). For each library, the

1085 “mean of 3 elements” was calculated as the mean knockdown of all three elements targeting each
1086 gene. The “best of 3 elements” represents the element with the best knockdown per each gene.
1087 g. Comparison of target gene knockdown across elements in dual-sgRNA library versus
1088 Dolcetto.
1089 See also Figure S1.
1090



1091

1092

Figure 2. CRISPRi effectors containing SID or MeCP2 domains have non-specific effects

1093 **on cell viability and gene expression.**

1094 a. Schematics of CRISPRi transcription repressor domains and general lentiviral expression
1095 construct used for all CRISPRi effectors.

1096 b. Experimental design to test effects of stable expression of each CRISPRi effector on growth
1097 and transcription in K562 cells.

1098 c. Growth defects of effector-expressing cells, measured as the \log_2 ratio of mCherry-negative
1099 (effector-expressing) to mCherry-positive (not effector-expressing) cells in each well. mCherry
1100 levels were measured for 19 days after pooling cells. Data represent mean \pm SD from three
1101 independent transductions of expression constructs. p -values are from an unpaired two-tailed t-
1102 test comparing D19 values for each sample to the D19 value for the "no plasmid" sample.

1103 Average percent growth defect per day is the \log_2 D19 value divided by the number of days,
1104 multiplied by 100 for a percent value.

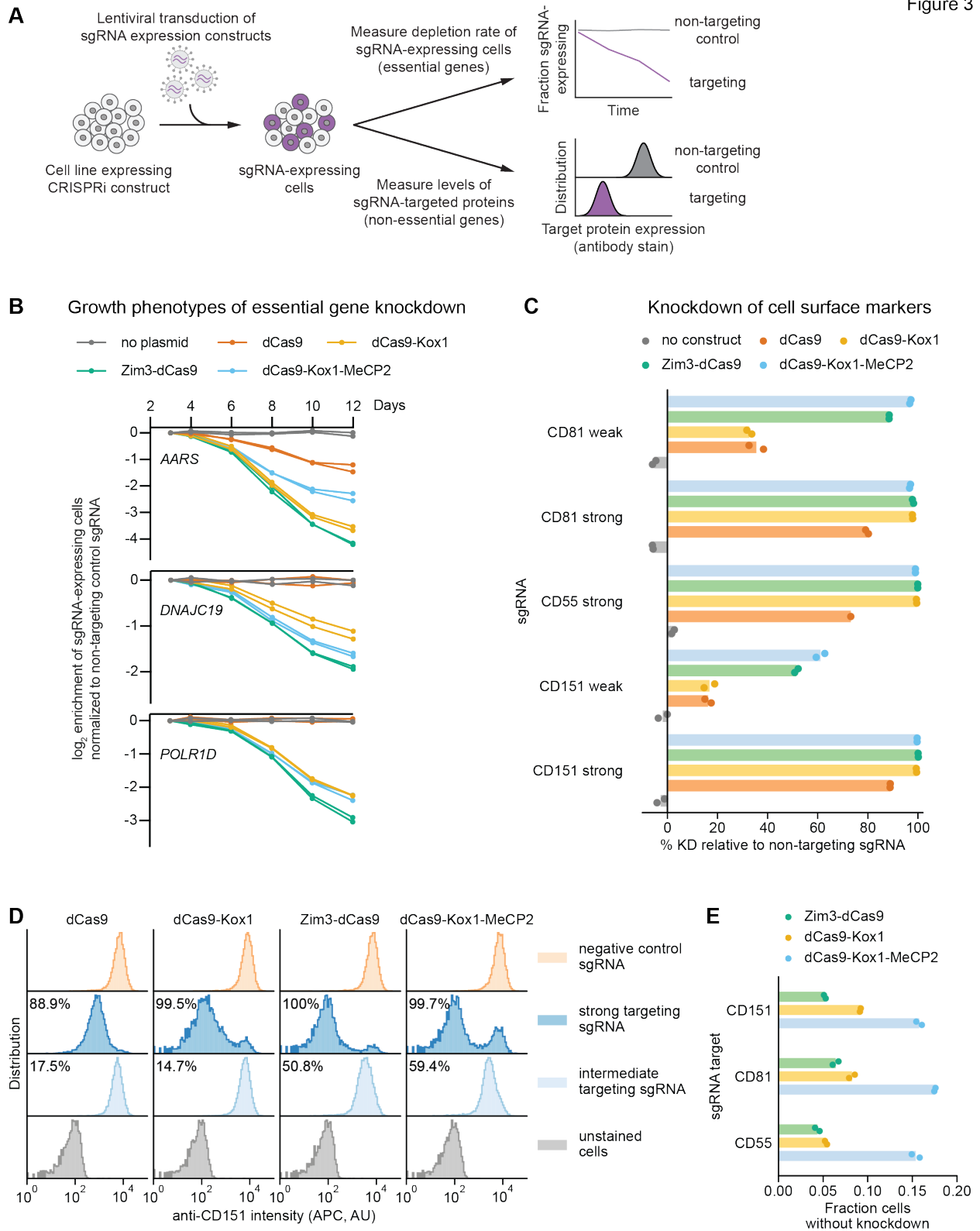
1105 d. Clustered heatmap of correlation of transcript counts from K562 cells expressing indicated
1106 CRISPRi effectors or a GFP control. Correlations across samples were calculated using
1107 normalized counts (reads per million) for all genes with mean normalized count >1 and then
1108 clustered using the Ward variance minimization algorithm implemented in *scipy*. r^2 is squared
1109 Pearson correlation. Data represent three independent transductions of expression constructs.

1110 e. Number of differentially expressed genes ($p < 0.05$) for cells expressing each effector versus
1111 cells expressing GFP only. p -values were calculated using a Wald test and corrected for multiple
1112 hypothesis testing as implemented in *DeSeq2*.

1113 See also Figure S2.

1114

1115



1116

1117

Figure 3. Zim3-dCas9 and dCas9-Kox1-MeCP2 mediate strongest knockdown.

- 1118 a. Experimental design to measure knockdown mediated by different CRISPRi effectors by
1119 delivering sgRNAs targeting either essential genes or cell surface markers.
- 1120 b. Depletion of K562 cells expressing essential gene-targeting sgRNAs and different CRISPRi
1121 effectors, measured as the ratio of mCherry-positive (sgRNA-expressing) to mCherry-negative
1122 (not sgRNA-expressing) cells in a given well. mCherry levels were measured for 12 days after
1123 transduction, starting on day 3. Data from two replicate transductions.
- 1124 c. Percent knockdown of cell surface markers by different CRISPRi effectors in K562 cells. Cell
1125 surface marker levels were measured on day 6 post-transduction by staining with an APC-
1126 conjugated antibody. Knockdown was calculated as the ratio of median APC signal in sgRNA-
1127 expressing cells and median APC signal in cells expressing a non-targeting control sgRNA after
1128 subtraction of background APC signal. Data from two replicate transductions. Cells expressing
1129 dCas9 and a strong CD55-targeting sgRNA are represented by a single replicate.
- 1130 d. Distribution of anti-CD151 signal intensity (APC) in individual cells from one representative
1131 transduction. Data from second replicate are shown in Figure S3b. Knockdown was quantified as
1132 in Figure 3c.
- 1133 e. Fraction of cells without observable knockdown despite expressing a strong sgRNA, as
1134 quantified from the fluorescence distributions.
- 1135 See also Figure S3.
- 1136
- 1137

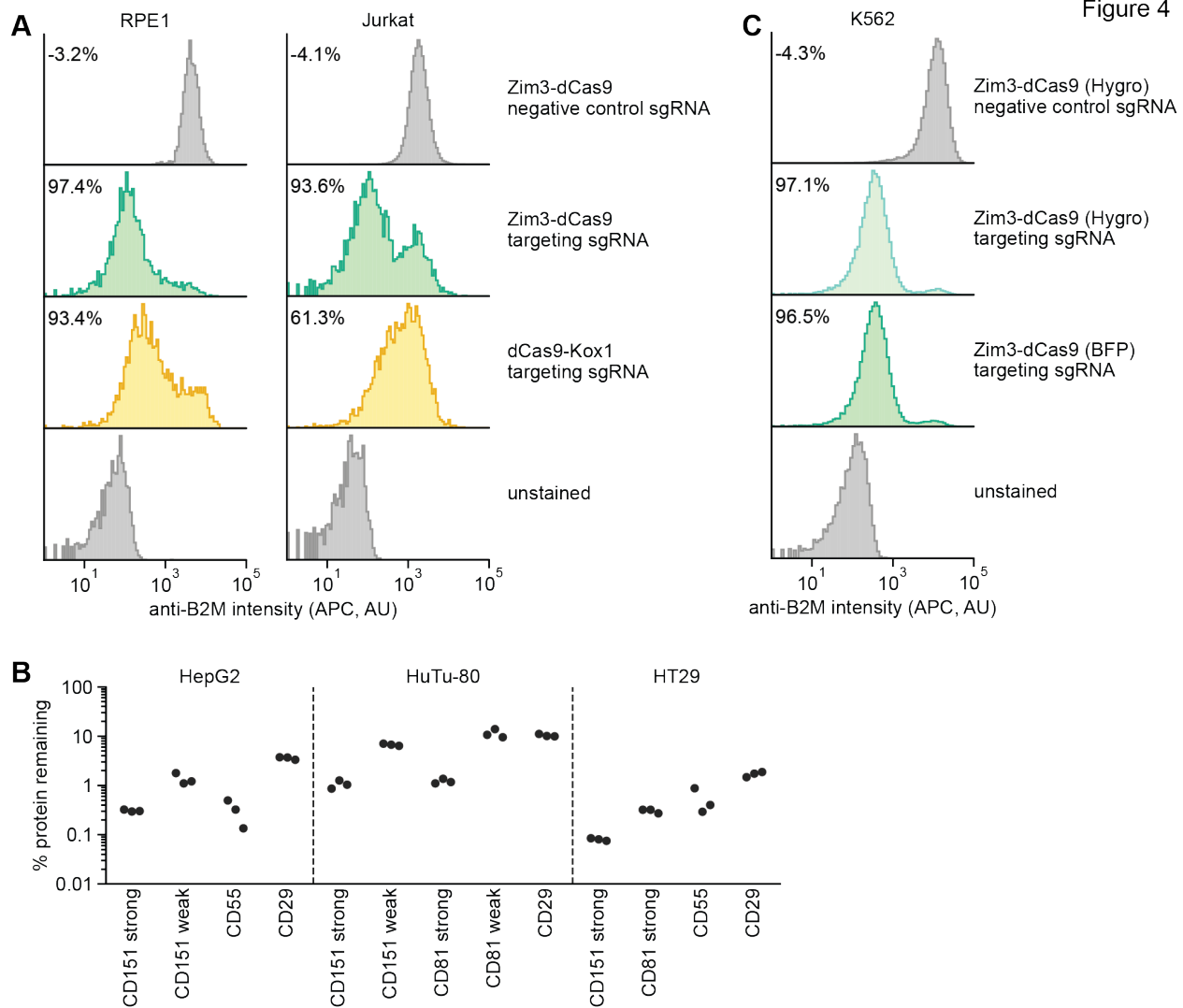


Figure 4

1138

1139 **Figure 4. Validation of a suite of optimized Zim3-dCas9 cell lines.**

1140 a. Distribution of anti-B2M signal intensity (APC) in individual RPE1 (left) and Jurkat (right)

1141 cells expressing indicated CRISPRi effectors and sgRNAs. Knockdown was calculated as the

1142 ratio of median APC signal in transduced (sgRNA-expressing) cells and median APC signal in

1143 non-transduced cells in the same well, after subtraction of background APC signal.

1144 b. Depletion of indicated cell surface markers in HepG2 (left), HuTu-80 (middle), and HT29

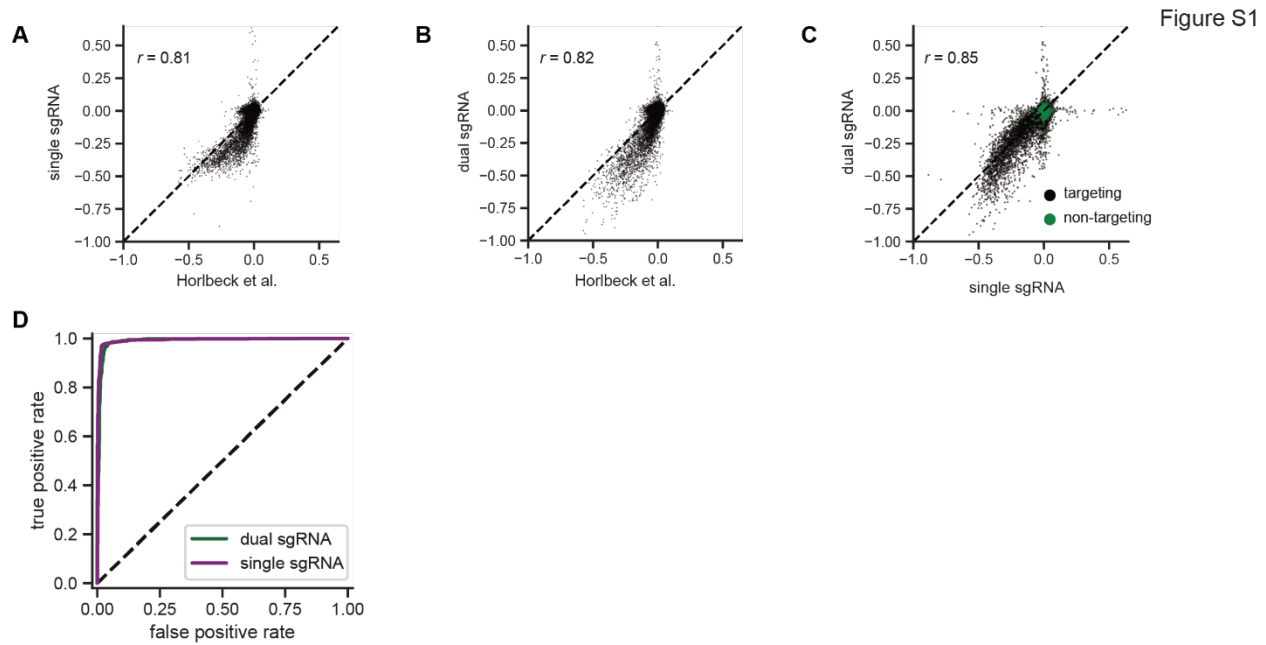
1145 (right) cells expressing Zim3-dCas9. Cell surface marker levels were measured 6-14 days post-

1146 transduction by staining with APC-conjugated antibodies. Knockdown was calculated as the

1147 ratio of median APC signal in sgRNA-expressing cells and median APC signal in cells

1148 expressing a non-targeting control sgRNA after subtraction of background APC signal.

1149 c. Distribution of anti-B2M signal intensity (APC) in individual K562 cells expressing indicated
1150 CRISPRi effectors and sgRNAs. The Zim3-dCas9 (Hygro) cell line was generated by
1151 transduction followed by hygromycin selection and does not express a fluorescent protein.
1152 Knockdown was calculated as in Figure 4a.
1153 See also Figure S4.
1154



1155

1156 **Figure S1. Additional comparisons of pilot single- and dual-sgRNA library screens.**

1157 a. Comparison of growth phenotypes for all elements between our pilot single-sgRNA library
1158 and Horlbeck et. al data, merged by gene name (n=20036 elements). Growth phenotypes are
1159 reported as γ (\log_2 fold-enrichment of T_{final} over T_0 , per doubling) and correlated between
1160 experiments ($r = 0.81$).

1161 b. Comparison of growth phenotypes for all elements between our pilot dual-sgRNA library and
1162 Horlbeck et. al data, merged by gene name (n=20036 elements). Growth phenotypes are reported
1163 as γ and correlated between experiments ($r = 0.82$).

1164 c. Comparison of growth phenotypes for all elements between our pilot single- and dual-sgRNA
1165 libraries, merged by gene name (n=21049 with 20036 targeting elements and 1013 non-targeting
1166 elements). Growth phenotypes are reported as γ and correlated between experiments ($r = 0.85$).

1167 d. Comparison of true and false positive rates in single element screens. “Positives” (n=1239
1168 elements) were defined as genes with a K562 CRISPRi growth screen p -value < 0.001 and $\gamma < -$
1169 0.05 (Horlbeck et al., 2016a), and “negatives” were defined as non-targeting control sgRNA
1170 pairs (n=1013 elements).

1171

1172

Figure S2

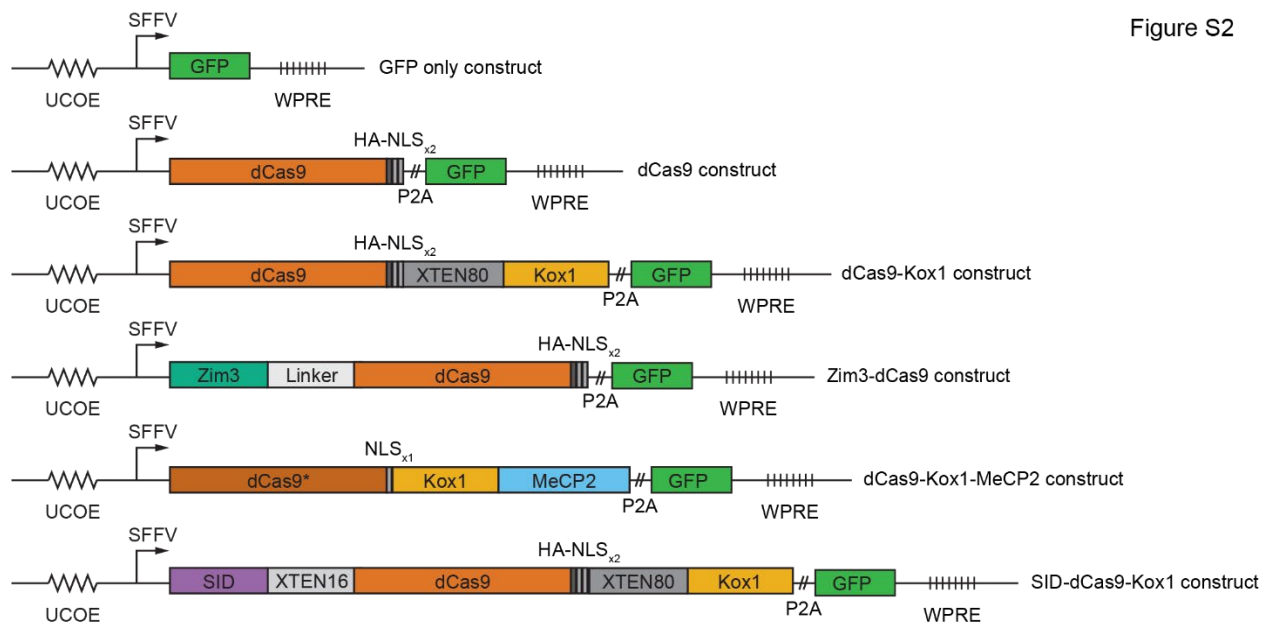
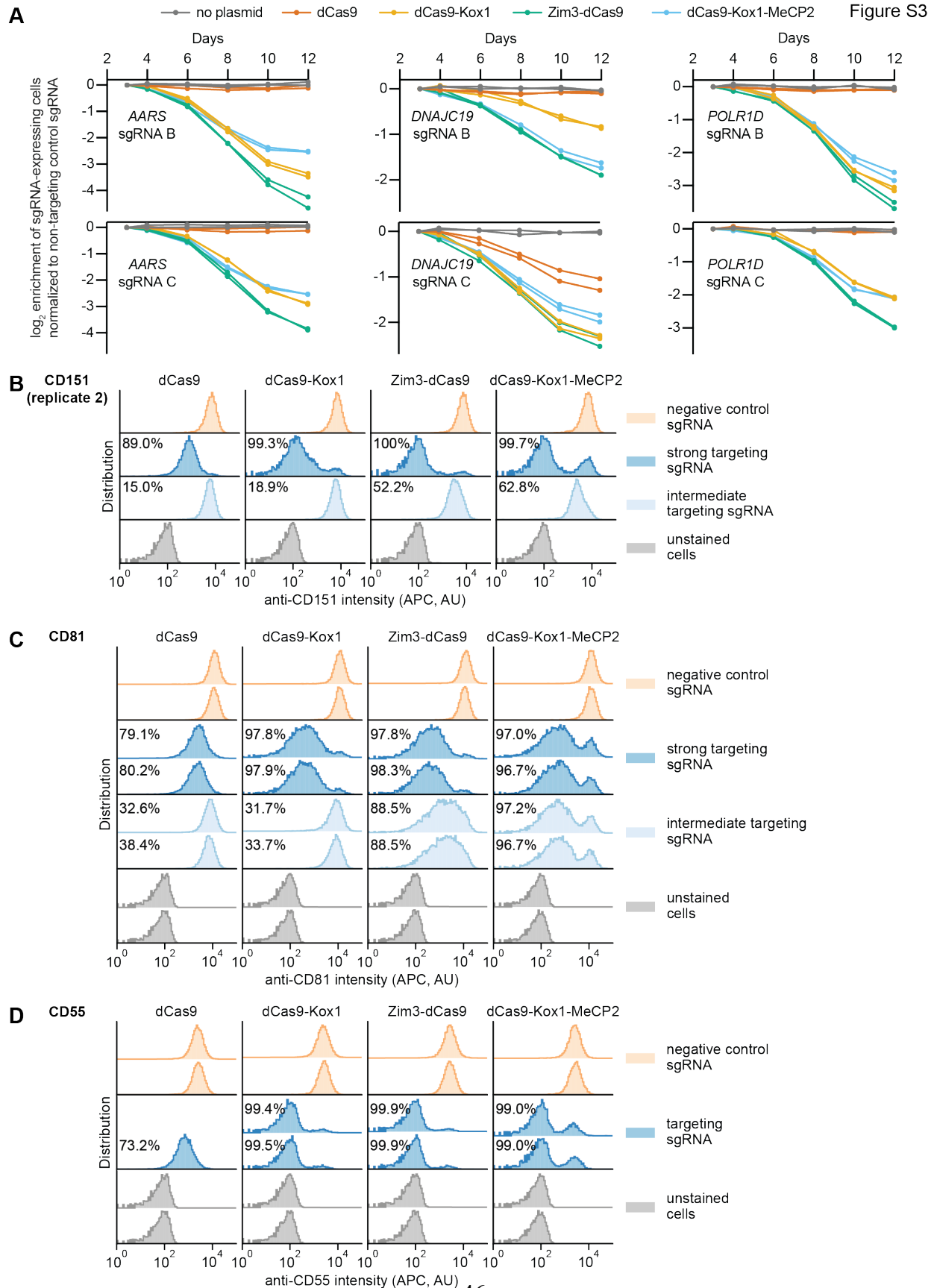


Figure S2. Design of constructs for CRISPRi effector expression.



1178 **Figure S3. Additional measurements of on-target activity of CRISPRi effectors.**

1179 a. Depletion of K562 cells expressing essential gene-targeting sgRNAs and different CRISPRi
1180 effectors, measured as the ratio of mCherry-positive (sgRNA-expressing) to mCherry-negative
1181 (not sgRNA-expressing) cells in a given well, as in Figure 3a. mCherry levels were measured for
1182 12 days after transduction, starting on day 3. Data from two replicate transductions.

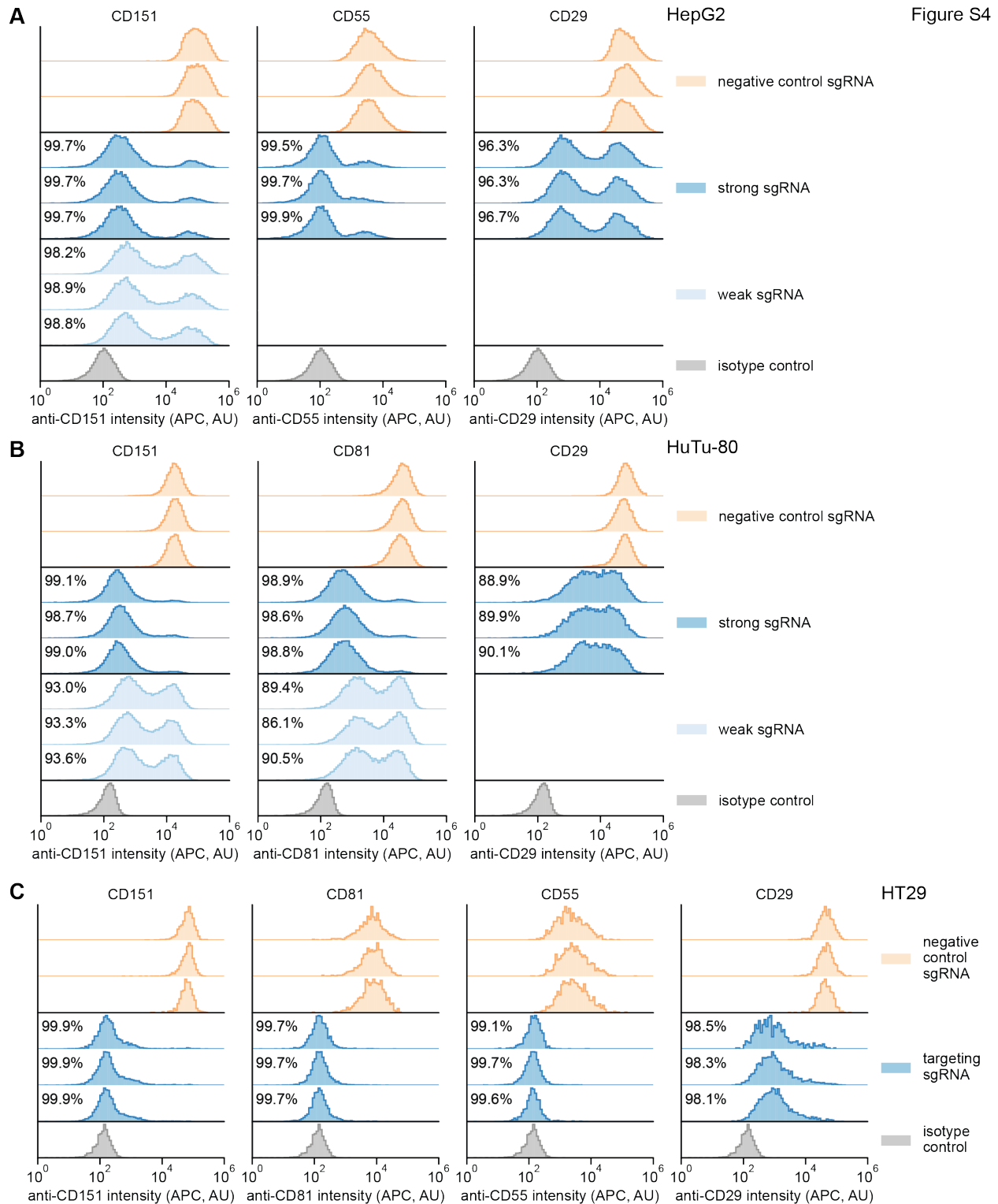
1183 b. Distribution of anti-CD151 signal intensity (APC) in K562 cells expressing indicated
1184 CRISPRi effectors from second replicate transduction. Knockdown was quantified as in Figure
1185 3c.

1186 c. Distribution of anti-CD81 signal intensity (APC) in K562 cells expressing indicated CRISPRi
1187 effectors from two replicate transductions. Knockdown was quantified as in Figure 3c.

1188 d. Distribution of anti-CD55 signal intensity (APC) in K562 cells expressing indicated CRISPRi
1189 effectors from two replicate transductions. Cells expressing dCas9 and the CD55-targeting
1190 sgRNA are represented by a single replicate. Knockdown was quantified as in Figure 3c.

1191

1192



1193

1194 **Figure S4. Single-cell distributions of knockdown in different Zim3-dCas9 cell lines.**

1195 a. Distribution of anti-CD151, anti-CD55, and anti-CD29 signal intensities (APC) in HepG2

1196 cells expressing Zim3-dCas9. Data from 3 independent transductions are shown. A weak

1197 targeting sgRNA was only included for CD151. For the isotype control, cells expressing the
1198 negative control sgRNA were stained with an APC-conjugated isotype control antibody. A single
1199 replicate is shown for the isotype control. Knockdown was calculated as in Figure 4b.

1200 b. Distribution of anti-CD151, anti-CD81, and anti-CD29 signal intensities (APC) in HuTu-80
1201 cells expressing Zim3-dCas9. Data from 3 independent transductions are shown. A weak
1202 targeting sgRNA was only included for CD151 and CD81. For the isotype control, cells
1203 expressing the negative control sgRNA were stained with an APC-conjugated isotype control
1204 antibody. A single replicate is shown for the isotype control. Knockdown was calculated as in
1205 Figure 4b.

1206 c. Distribution of anti-CD151, anti-CD81, anti-CD55, and anti-CD29 signal intensities (APC) in
1207 HT29 cells expressing Zim3-dCas9. Data from 3 independent transductions are shown. Only
1208 strong targeting sgRNAs were included. For the isotype control, cells expressing the negative
1209 control sgRNA were stained with an APC-conjugated isotype control antibody. A single
1210 replicate is shown for the isotype control. Knockdown was calculated as in Figure 4b.

1211

1212

1213

1214 **Supplementary Tables**

1215 Table S1. Dual- and single-sgRNA libraries used for preliminary comparison.

1216 Table S2. Aggregated CRISPRi sgRNA performance across screens.

1217 Table S3. Finalized dual-sgRNA CRISPRi libraries.

1218 Table S4. List of integration barcodes.

1219 Table S5. Dolcetto versus dual-sgRNA Perturb-seq comparison.

1220 Table S6. Description of plasmids.

1221 Table S7. Sequences of sgRNAs used for individual validation.

1222 Table S8. Dual-sgRNA CRISPRa libraries.

1223

1224 **Supplementary Notes**

1225 Supplementary Note 1. Protocol for cloning dual-sgRNA libraries.

1226 Supplementary Note 2. Protocol for sample preparation and Illumina sequencing of dual-sgRNA
1227 libraries.

1228 Supplementary Note 3. Protocol for arrayed cloning of dual-sgRNA constructs.

1229 Supplementary Note 4. Protocol for generation of CRISPRi cell lines.

1230